April 2007

Design of a Mechanical Model for Pulsatile Aortic Flow

Joseph T. Guzman
Worcester Polytechnic Institute

Koren E. Roach
Worcester Polytechnic Institute

Lisa E. Currier
Worcester Polytechnic Institute

Matthew D. Rosi
Worcester Polytechnic Institute

Design of a Mechanical Model for Pulsatile Aortic Flow

A Major Qualifying Project Report:

Submitted to the Faculty

Of the

WORCESTER POLYTECHNIC INSTITUTE

In partial fulfillment of the requirements for the

Degree of Bachelor of Science

by

Joseph Guzman Lisa Novoson Koren Roach Matthew Rosi

Date: April 26, 2007

Advisor:

Professor Brian J. Savilonis

Table of Contents

Authorship

Section:	Written By:
Chapter 1: Introduction	Lisa Novoson
Chapter 2: Literature Review	Lisa Novoson
Chapter 3: Project Approach	Joseph Guzman
Chapter 4: Design	Joseph Guzman & Matthew Rosi
Chapter 5: Methods	Matthew Rosi
Chapter 6: Results	Koren Roach
Chapter 7: Analysis and Discussion	Koren Roach
Chapter 8: Conclusions	Koren Roach & Lisa Novoson
Chapter 9: Recommendations	Lisa Novoson

Acknowledgements

We would like to acknowledge the following people, without whom this project could not have been completed.

Professor Brian J. Savilonis- For his guidance, direction, and advice throughout the project.

Professor Norton- For his help with modeling the cam using Dynacam software.

Professor Holly Ault- For her assistance in modeling the mechanical parts in ProEngineer and Solidworks.

MuraliMurugavel Swathanthira Kumar- For his assistance with LabVIEW, MATLAB, and data acquisition.

Neil Whitehouse- For his assistance in the manufacturing of the mechanical parts.

Marc Guillemette- For his aid with setting up the pressure transducers.

Abstract

Worldwide, millions of people suffer every year from at least one type of cardiovascular disease. The most common type of these diseases is atherosclerosis, which is the build up and hardening of excess tissue, inflammatory cells, and lipids on the arterial wall in one or multiple arteries or veins. Atherosclerosis can exist asymptomatic in the body for years, only being detected when it poses a major health hazard. Vessels can become up to 80% occluded before the subject will feel any adverse affects, which may include stroke or myocardial infarction

This project focuses on the need for the development of a method for the detection of early stage atherosclerosis. The study will focus specifically on the feasibility of non-invasively detecting plaque through blood pressure and flow analysis.

The design of the mechanical model depended on the flow rate waveform produced by blood flow in the abdominal aorta. In producing the flow curve, it was important that the design capture enough harmonics of the curve to properly interpret any changes in frequency response in a diseased artery.

The physical flow from the mechanical model was produced by a cam and piston pump. The dimensions for the shape of the cam were calculated based on the abdominal flow curve. The curve was digitized and imported into DynaCam software.

The pump system consisted of a water tight piston head with an O-ring connected to a follower. The follower was spring loaded to maintain contact with the rotating cam. The cam was powered to rotate at 60 rpm, equivalent to a heart rate of 60 bpm.

To match the compliance of abdominal and iliac arteries, 1/2” and 1” Penrose tubing was used. Plaque buildup was simulated with Loctite® medical adhesive glue in the iliac regions of the models.

The flow produced by the pump was measured with pressure transducers. The acquired data was inputted into a LabView program and analyzed with the Fast Fourier Transform (FFT). The frequencies present in the healthy model artery were compared to those present in the data of the diseased state.

Through our study we were able to discover that the pressure readings gathered suggests that minor occlusions on the order of 10% blockage of cross sectional area do produce statistically significant changes in pressure, which become more significant with increased blockage

This suggests that one should assess the feasibility of a non-invasive procedure to measure changes in harmonics of the pressure waveform in order to detect early stages of atherosclerosis.

Table of Figures

Table of Tables

Part I: Proposal

Chapter 1: Introduction

1.1 Cardiovascular Disease and Atherosclerosis

Worldwide, millions of people suffer every year from at least one type of cardiovascular disease [1]. Cardiovascular disease refers to the group of diseases related to either the heart or arterial system. The most common type of these diseases is atherosclerosis, which is the excess build up of plaque in one or multiple arteries or veins. Atherosclerosis is a serious disease that can result in the hardening of the arteries. If gone undetected it can restrict and occlude normal blood flow. Severe cases of the disease can result in stroke, heart attack, and death.

1.1.1 Anatomy specifics

Atherosclerosis is the buildup of excess tissue, inflammatory cells, and lipids on the arterial wall [2]. Arteries themselves are comprised of three layers; the innermost being the tunica intimae, followed by the internal elastic lamina, and the outermost the tunica adventitia. A schematic of the vessel can be seen in Figure 1. During the progression of the disease, the deposit continues to accumulate, pushing the wall of the affected vessel out and expanding all three layers. This phase of the disease is called positive remodeling because the vessel diameter increases to allow for the buildup while maintaining normal blood flow [2].

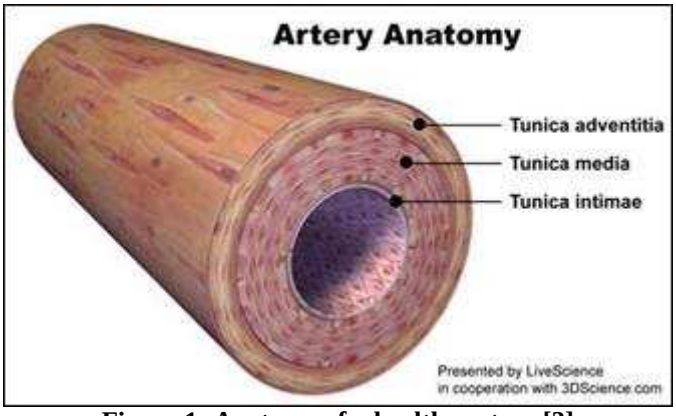

Figure 1: Anatomy of a healthy artery [3]

The second phase of the disease occurs when the vessel wall can no longer expand to compensate for the plaque. At this time, the plaque encroaches into the lumen (inner space of the vessel), and begins to restrict blood flow. A schematic of this phase can be seen in Figure 2. Atherosclerosis can be asymptomatic during the remodeling phase of the disease. Detection usually does not occur until the subject has a noticeable lack of blood to an appendage, or experiences angina, myocardial infarction, or a stroke.

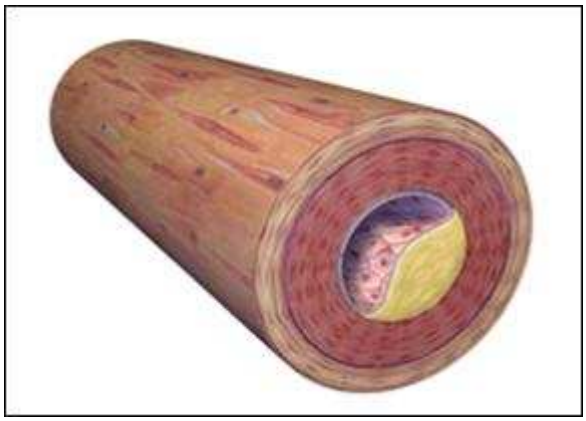

Figure 2: Anatomy of a diseased artery [3]

Ischemia, or a restricted blood supply often does not occur until the occlusion of the vessel lumen is at 80-90%. This value can be lower depending on the demand for blood. Ischemia of the heart muscle can lead to angina and heart attack. Pieces of the accumulated mass are also prone to breaking off the vessel wall and lodging in a smaller vessel, causing stroke in severe cases [2].

Susceptibility to atherosclerosis can be genetic, or based on weight and level of daily activity. Natural cholesterol producers can have a higher occurrence of atherosclerosis due to their body chemistry. Similarly, people with diets high in cholesterol, or obese subjects are also more prone to the lipid deposits. Plaque build up is common in the medium pressure arteries of the body. The heart, aorta, and abdominal aorta are generally too high pressure to allow for cell adhesion or lipid deposition on the arterial wall.

Common places for atherosclerosis are the iliac arteries, and the coronary arteries. Plaque buildup in the coronary arteries leads to a specific type of cardiovascular disease known as coronary heart disease. This occurs when an artery supplying the heart with

oxygenated blood is occluded. It is estimated that over 13,000,000 Americans were diagnosed with coronary heart disease in the year 2003 [1].

1.2 Current Treatment

The idea for treating atherosclerosis came from Charles Dotter in the 1960's [4]. Over the years, there have been a number of procedures used for the treatment of atherosclerosis. Current methods include balloon angioplasty, implantable vascular stents, and vessel grafts. The following section will briefly describe each method.

1.2.1 Angioplasty

Angioplasty is the method by which the diseased artery is widened by mechanical force. This is generally done with a balloon tipped catheter. The catheter is inserted in the femoral artery in the groin and snaked up the abdominal and thoracic aortas to the diseased site. The balloon tip is then inflated to 9000-13500 mmHg to expand the vessel [5]. After expansion, the balloon is deflated and removed.

An advantage of this technique is that it is not considered a surgical procedure [6]. This is a minimally invasive treatment that does not require major surgery or general anesthesia. In most cases, anti-coagulation and mild pain medicines are the only medications administered to the patient.

Angioplasty exists as a temporary solution to occluded vessels. Its use as a permanent fix is limited by the high occurrence rate of vessel restenosis. Restenosis is the re-closing of the affected artery. Once expanded, the vessel does not remain open long term. Another disadvantage of this method is the possible dislodging of plaque during the procedure. Dislodged plaque can float in the blood stream and potentially cause emboli depending upon where it gets stuck. Angioplasty is still used today, but it is chosen secondary to cardiac stents.

1.2.2 Stents

Currently, the leading treatment for atherosclerosis is the implantation of vascular stents. This method has experienced tremendous success and is praised for its minimally invasive nature and quick recovery times. In an attempt to improve upon the traditional

balloon angioplasty, Charles Dotter introduced the idea of endovascular stents in 1964. After some time, he demonstrated their feasibility in the revascularization of diseased arteries in 1983 [4].

A stent is a wire mesh tube inflated in the artery using traditional balloon angioplasty used to prop open the vessel long term. An illustration of the procedure can be seen in Figure 3.

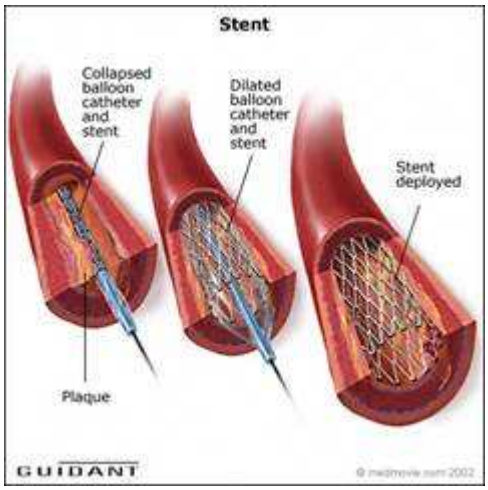

Figure 3: Progression of stent delivery [8]

There are more than 50 types of stents that have been approved for medical use by the FDA [7]. The first stents on the market were bare metal, usually 316L stainless steel. As technology has advanced, the nature of stents has progressed as well. Cardiac stents have evolved from these bare metal designs to incorporate coatings and drugs that aid in maintaining an open vessel.

One problem with the bare metal stents is the rate of restenosis. Smooth muscle cells can adhere, proliferate, and overgrow the struts of the stent. In addition to more accumulating plaque, the artery can become narrowed even after treatment. An image of restenosis can be seen in Figure 4.

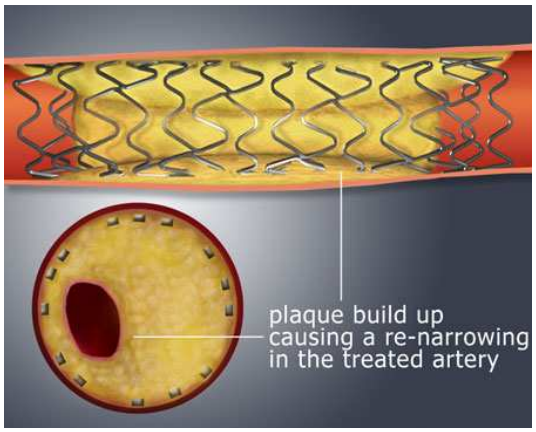

Figure 4: Restenosis of vessel after stent implantation [9]

Another disadvantage to bare metal stents is the potential for thrombosis. Platelets and blood cells adhere and clot on the surface of the stent, accumulating until the blood flow detaches the mass. This mass can lodge in arteries causing embolisms and possible stroke and death.

The rate of restenosis and emboli causing thrombosis led researchers to develop drug-eluting stents (DES). DES are usually bare metal stents coated with a thin layer of polymer that releases drug over time. These polymers can degrade as the drug is delivered, ensuring that the inflammation of the vessel is kept to a minimum to prevent restenosis. The current drug used on many market approved stents prevents cell proliferation, and thus overgrowth of the stent by unwanted cells.

Though this method has been praised, recent clinical data has indicated that there are still concerning problems with these devices. Long term data from clinical studies suggest that even the DES cause possible thrombosis.

1.2.3 Grafts

Vessel grafting is a traditional method for treating blocked arteries. Usually the last option for patients with atherosclerosis, this involves a major invasive open heart surgery. In addition to the heart surgery, surgeons have to perform an additional surgical procedure to procure the autograft vessel. Commonly used vessels are the saphenous veins of the legs and thighs.

There are several drawbacks to this procedure. The first is that it is much more invasive than both angioplasty and vascular stents. Another drawback is the compliance

between the grafted vein and the native tissue. Because the vein has different elastic properties from the coronary arteries, when replacing an artery, the graft usually undergoes additional stresses not normally experienced by a vein. In some cases this compliance mismatch can cause bulging of the graft or aneurisms.

1.3 Early detection

The symptoms of atherosclerosis are typically not detected until serious complications arise and by this stage, reversing the disease process is quite unlikely. A clinical technique to detect atherosclerosis in its beginning stages, preferably in a noninvasive method, might prevent or reverse the progression of the disease and prevent the occurrence of serious complications. Currently, imaging techniques focus on lesions, while other techniques measure changes in the mechanical properties of the arteries and the affect atherosclerosis has on the hemodynamics therein. The forms of non-invasive techniques available today, most notably, include impedance plethysmography, digital subtraction angiography, nuclear magnetic resonance, and ultrasound.

1.3.1 Existing Techniques for Early Detection

A dissertation by S. Kolluri evaluated a non-invasive technique for early detection of atherosclerosis using an impedance plethysmograph. A three-channel impedance plethysmograph was developed that allowed for simultaneous measurement of change in impedance signals in three different places. The progress of the disease was studied noninvasively in the left and right femoral arteries and poplitial arteries, carotid artery, left brachial artery and the abdominal aorta of 20 male cynomolgus monkeys. A pressure cuff and a pair of electrodes were wrapped around the upper left leg of the monkey; another electrode was placed distal to the pressure cuff and another on the upper arm as a reference. These three points were used to measure impedance pulses simultaneously. The pressure in the cuff was changed from 200mmHg to 20mmHg and these results were used to evaluate arterial volume change. The progression of the disease was monitored using the characteristics of arterial volume change vs. cuff pressure. The study found that the original, well defined peak changed to a flatter characteristic with an increased period as time progressed for monkeys on high cholesterol diets. Monkeys on the control diet

did not have any flattening of the curve over time. Results also showed a decrease in peak compliance with a shift to the left during the progression of the disease [10].

Digital Subtraction Angiography (DSA) is a technique used to visualize blood vessels in the body. The original technique, angiography, involves injecting a radiographic contrast agent into the blood vessel and taking radiographs at appropriate time intervals. DSA allows the angiographic images to be captured digitally along with the subtraction of bony and soft tissue.

During a study by M. Ogawa *et al,* WHHL rabbits were injected with ^{18}F-FDG to determine if it builds up in atherosclerotic lesions. This study found that the accumulation of ^{18}F-FDG in the lesions is caused by macrophages. Since macrophages play a key role in the rupture of plaque build-up, ^{18}F-FDG PET imaging would be an effective means for detecting vulnerable plaques and determining the risk of plaque rupture [11].

MR imaging was shown to characterize asymptomatic carotid artery plaques in a study by Honda *et al*. Intraplaque hemorrhage and thin fibrous caps were also found, which indicates a risk of plaque rupture. MR imaging also holds the potential to reveal intraplaque hemorrhage or necrotic core that may cause ishecmic attack and help to produce possibilities for future therapeutic strategies [12]. A magnetic resonance angiography (MRA) study using a single injection, five-station protocol demonstrated an accurate display of the arterial vasculature throughout the body. This study also used a limited number of regional DSA examinations, and found that the results of the MRA were sufficient to serve as a non-invasive alternative to DSA [13].

Nuclear magnetic resonance (NMR) spectroscopy is a technique used to obtain electronic, chemical, physical and structural information about a molecule. Additionally, NMR can provide detailed information on biological molecules in a solution and their three-dimensional structure. NMR spectroscopy was used in a study by Miyazaki to investigate circulating malondialdehyde-modified low-density lipoprotein (MDA-LDL) levels. This study found that endothelial function may be impaired by the circulating MDA-LDL, which may have a large impact on the pathogenesis of atherosclerosis [14].

Ultrasound is a means of visualizing the size, structure and presence of any lesions for muscles, tendons, and many internal organs. A study by Atkov *et al* found that ultrasound has the capability to detect the dysfunction of endothelial cells, and that this

dysfunction, when present in patients with familial hypercholesterolemia is a risk factor for atherosclerosis [15].

1.3.2 Lack of Existing Techniques

Though the aforementioned techniques have been used in the detection of early atherosclerotic plaque, there are still no highly dependable methods. Though the invention of vascular stents was seen to be one of the biggest achievements in cardiovascular medicine, it is still necessary to research methods of early prevention.

Atherosclerosis can exist asymptomatic in the body for years, only being detected when it poses a major health hazard. Vessels can become up to 80% occluded before the subject will feel any adverse affects. If left undetected, there is a possibility that when the problem becomes noticeable, the resulting stroke or myocardial infarction will have already been fatal.

Chapter 2: Literature Review

2.1 Anatomy

To fully understand atherosclerosis, and the need for early detection, one must first understand the anatomy of the affected areas. The cardiovascular system is composed of the arteries and veins that run throughout the body, and the heart, which supplies blood to the vessels. This section will detail the areas of the system relevant to creating a model for examining changes in blood flow.

2.1.1 Abdominal Aorta and Iliac Arteries

The abdominal aorta, or aorta abdominalis, is part of the aorta, the largest artery found in the vascular system. The aorta connects to the left ventricle of the heart and supplies the entire body with oxygenated blood. The aorta travels down the body cavity from the heart and becomes the thoracic aorta. After passing the diaphragm, the thoracic aorta becomes the abdominal aorta, which then splits to form the iliac arteries. The abdominal aorta is responsible for the blood supply to the abdominal and pelvic organs

and the muscles and tissue of the legs [16]. A diagram depicting the abdominal aorta and iliac arteries can be seen in Figure 5.

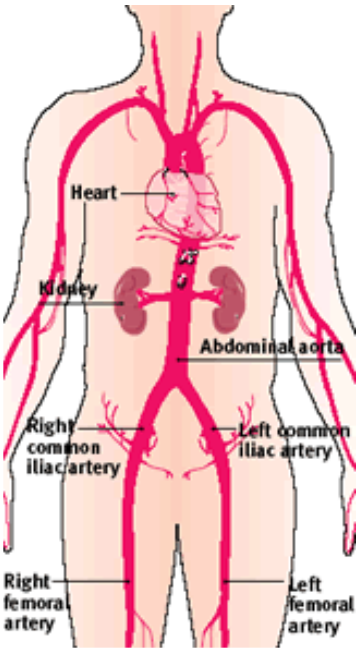

Figure 5: Cardiovascular system [17]

The abdominal aorta has many branches, as it supplies the blood to the lower half of the body. Common branches are the inferior phrenic, celiac, mesenteric, renal, gonadal, lumbar, median sacral, and iliac. The general characteristics of the abdominal aorta vary with the sex and age of the subject. Commonly the artery is approximately 20mm in diameter, with a wall thickness of 3-5 mm.

The iliac arteries are the terminal branches of the abdominal aorta. As seen in Figure 5, the iliac arteries and their branches are paired (each person has left and right vessels). These supply the oxygenated blood to the left and right legs and lower portions of the body. Similar to the abdominal aorta, size and characteristics of these arteries can vary with height, age, sex, and genetics. Normal common iliac arteries are approximately 4cm long in adults and 10mm in diameter.

The iliac arteries are common sites for atherosclerotic plaque buildup, specifically at the branching site. The change in pressure and flow in this region can lead to increased deposition of inflammatory cells and lipids. Because this is a potential site for

atherosclerosis, researchers have designed modified iliac stents to treat this specific area of diseased arteries [18].

2.1.2 Heart and Blood Characteristics

The heart is the primary organ of the cardiovascular system, supplying blood and oxygen to the body. It is a complex pump, synchronized with electrical signals. It has four chambers, two atria and two ventricles. The left ventricle attaches to the aorta, which, as mentioned previously, is the largest artery in the body. The left ventricle supplies blood to the body. The right atrium receives the blood returning from the veins in the body via the superior vena cava. The blood then passes into the right atrium, from which it travels to the lungs to receive more oxygen. The blood returns via the pulmonary vein into the left atrium, from which it passes through the mitral valve into the left ventricle. Figure 6 depicts the anatomy of a healthy heart.

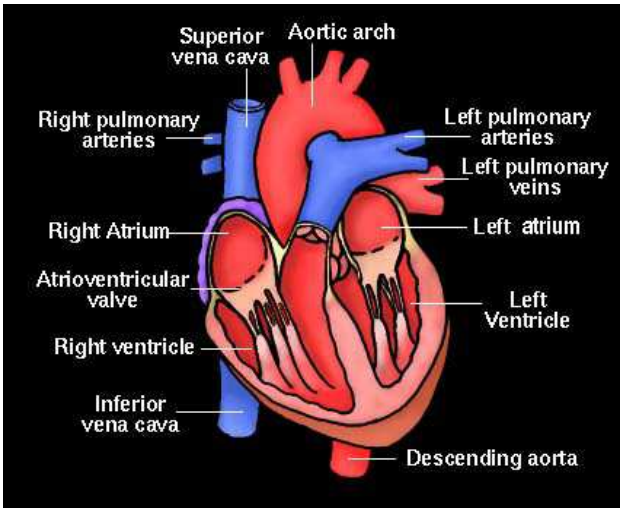

Figure 6: Anatomy of the heart [19]

The pumping of the heart creates a pulsatile flow in the vascular system. The pressure to supply the body with blood is broken into two parts, the systolic and diastolic pressures. Systolic blood pressure is the pressure in the vascular system when the ventricles of the heart are contracting. This value for a healthy body is around 120 mm Hg. The diastolic pressure is the pressure in the vascular system when the ventricles are relaxing. This constant pressure prevents the vessels from collapsing or experiencing backflow of blood. Normal values for this pressure are approximately 80 mm Hg.

The blood itself has many responsibilities. Primarily it regulates gas exchange in the body, supplying the cells with oxygen and removing the carbon dioxide wastes. It also circulates nutrients, hormones, and immune cells. Physically, blood is a suspension of cells in plasma. The cells are erythrocytes, leukocytes, and platelets. The plasma consists of gasses, salts, proteins, lipids and carbohydrates. The coefficient of viscosity for normal blood at 37°C is 3.5 centipoids (cP) or 0.0027 Ns/m^2 [20]. This number can be affected by the number and types of cells in suspension, and the temperature of the system.

2.1.3 Characteristics of Pulsatile Flow

The heart produces a signature type of flow through the vascular system. The pulse is created by the de- and re-polarization of the atria and ventricles. Seen in Figure 7 is the the electrical signal of a heart's pusatile flow as detected by an electrocardiogram (ECG). The P wave is the depolarization of the atria, the QRS is the depolarization of the ventricles, and the T wave represents the repolarization of the ventricles.

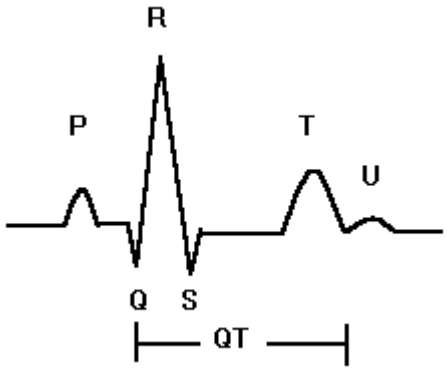

Figure 7: ECG signal of a heart beat [21]

This electrical synchronization leads to the pulsatile flow in the vascular system. The flow pattern can be characterized by a repeating curve, as seen for the abdominal aorta and iliac arteries in Figure 8. The high peaks represent the systolic pressure as the ventricles of the heart contract. The minimum of the curve signifies the diastolic pressure retained in the arteries.

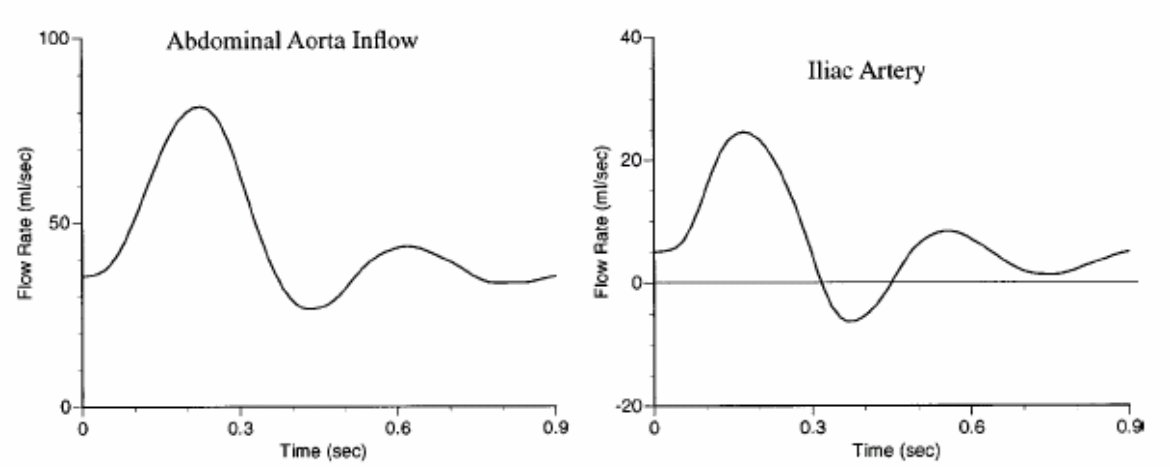

Figure 8: Flow rate curves for abdominal aorta and iliac arteries [22]

2.2 Pumps

2.2.1 Types of pumps

A pump is a device used to move liquids or gasses through a tube or pipe. This is done by using pressure differential; the gasses and liquids are moved from lower pressure to higher pressure. Pumps are needed when it is necessary to move a liquid or gas against the grain. There are many different pumps for moving liquids or gasses against the pressure gradient, all of which possess different methods for moving the material. The two main types of pumps are centrifugal and positive displacement pumps.

Centrifugal pumps are very simple pieces of machinery. The main idea behind this type of pump is that electricity will be converted by an electric motor into velocity or kinetic energy. This kinetic energy or pressure is then transferred by the pump into the liquid to increase the pressure. This energy change occurs in two main parts of the pump, the impeller and the volute. The impeller is the rotational part of the pump, composed of vanes, and is responsible for converting the electricity into kinetic energy. The volute is the stationary part of the pump and is responsible for converting kinetic energy into pressure. This transformation of energy occurs in a very specific manner. The liquid first enters the pump suction, and then travels to the eye of the impeller. The impeller then rotates and during this rotation it spins the liquid. During this the liquid that is located in the spaces between the vanes is spun outward while centrifugal acceleration is passed on. A low pressure area at the eye is created as the liquid leaves the eye. This low pressure

allows for more liquid to enter the pump inlet. There are three different types of centrifugal pumps: radial flow, mixed flow, and axial flow. In a radial flow pump the pressure is completely developed by the centrifugal force. In a mixed flow pump pressure is developed by centrifugal force and by the lift of the impeller vanes on the liquid. In an axial flow pump pressure is developed by the lifting of the vanes of the impeller on the liquid.

Positive displacement pumps are very different from centrifugal pumps. They work by having an object push a liquid out of a chamber. Positive displacement pumps are also subdivided into two other groups, single rotor and multiple rotors. Single rotor pumps only have one object pushing the liquid while multiple rotors have many. Some types of single rotor pumps include: vane, piston, flexible member, single screw and progressing cavity. Vane pumps use blades or another suitable object, which cooperate with a dam to draw fluid into and out of the fluid chamber. A piston pump has a piston reciprocating within cylinder and operating port valves which draws fluid in and out of the chamber. The flexible member pump has a flexible member pumping and sealing the fluid. A single screw pump has the fluid carried between rotor screw threads as they mesh with the internal threads. A progressing cavity pump has the fluid carried between a rotor and flexible stator. Examples of multiple rotor pumps are: gear, lobe, circumferential piston and multiple screws. In a gear pump the fluid is pumped by the meshing of the gear teeth. In a lobe pump the fluid is pushed between rotor lobes which work together to provide continuous sealing between the inlet and outlet. The circumferential piston and the multiple screw pumps are similar to the single rotor ones, but contain multiple rotors.

2.2.2 Cam and Piston

By combining the positive displacement method with a cam, one is able to recreate a pulsatile flow. The pressure and flow curves of the abdominal aorta and iliac arteries can be broken down into harmonics, and a series of sine and cosine waves. These waves can be recreated by the use of a cam. A cam is a rotating projection that can be attached to a follower. A round cam will produce a perfect sine wave. A picture of a cam follower system can be seen in Figure 9.

Figure 9: Cam and follower system [23]

2.3 Methods of Waveform Analysis

2.3.1 FFT

A typical waveform plot uses time as the independent variable, but the frequency spectrum can also be plotted. This involves plotting the frequency as the independent variable and the amplitude of each frequency component is the dependent variable. This allows the frequencies present in a signal to be identified quickly and easily. Fourier analysis is the process used to determine the frequency of a known waveform. This is also referred to as harmonic analysis.

A fast Fourier transform (FFT) uses an efficient algorithm to calculate the discrete Fourier transform (DFT) and the inverse. This computer algorithm uses acquired data to calculate the frequency spectrum .The DFT is defined by the following formula:

$$X_k = \sum_{n=0}^{N-1} x_n e^{-\frac{2\pi i}{N} nk}$$

where $k = 0,\ldots,N-1$ and i is the imaginary unit ($i^2 = -1$). DFT is used to analyze frequencies in a signal sample, solve partial differential equations and perform other operations. The discrete sample is typically taken by an analog to digital (A/D) converter which is connected to an electronic spectrum analyzer driven by a microprocessor or a computer. The sums are evaluated by the computer or microprocessor, often with the use of the fast Fourier transform algorithm. The FFT algorithm applies only when N is a power of two ($N=2^m$, m is an integer). Typically, the number of calculations required to calculate these sums is proportional to N2, but when the FFT algorithm is used, the number is proportional to Nlog2N. This allows for fewer calculations when N is large

[24]. If N is not a power of two, algorithms can compute the DFT, but at a much slower speed than that of FFT [25].

Fourier transforms are often used to find the frequency components of a signal convoluted with a noisy time domain signal. If the frequency components are difficult to determine in a noisy signal sample, FFT can convert the data to the frequency domain. The resulting frequency plot will clearly demonstrate the amplitudes of the original data as two drastic peaks on the graph [26].

FFT is a form of Frequency Domain Analysis and used for breaking up signal samples. A signal sample is normally not a sine or cosine wave, but a combination of different sin and cosine waves with varying amplitudes or frequencies. Fourier's theorem states that "…any waveform in the time domain can be represented by a weighted sum of sine and cosine waves." In the figure below, the sum waveform appears in the frequency domain as the phase and amplitude values at each frequency component (f0, 2f0, 3f0) [27].

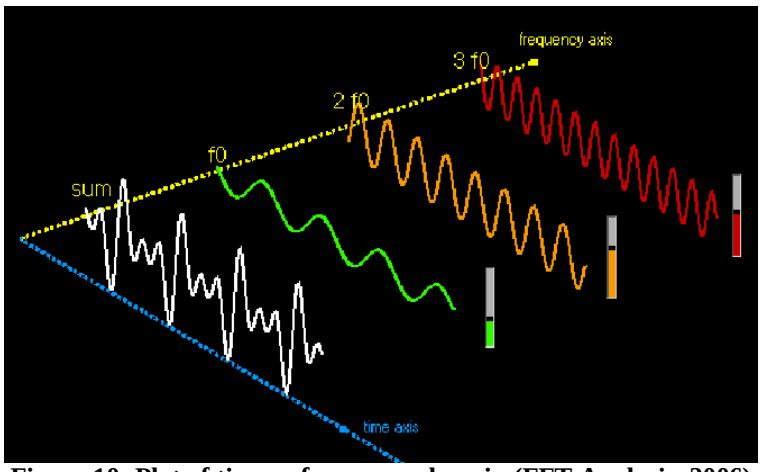

Figure 10: Plot of time v. frequency domain (FFT Analysis, 2006)

Chapter 3: Project Approach

It has been stated that pressure readings taken of the abdominal aorta, when the iliac branches are partially blocked, are not statistically significant and only become significant when the branches are 75-90% occluded. Many studies have been conducted to determine if minimal blockages will affect the pressure found in the abdominal aorta. These studies looked to determine the feasibility of a noninvasive method for early

detection of minimal blockages. These studies have found that this noninvasive method is not feasible, since the pressure readings only become statistically significant when the patient has a large blockage and is experiencing symptoms.

The goal of the project was to develop a mechanical model that mimicked the flow through the abdominal aorta under different degrees of blockage. Through the use of this model readings were gathered to determine that harmonic analysis of the pressure readings were statistically significant after only 10-20% blockage of the iliac branch. Multiple trials were conducted to provide enough data to determine statistical significance. Data was gathered that would disprove that idea that the pressure readings were only statistically significant when there was a large blockage.

Chapter 4: Design

4.1 The Design Process

The production of a pump that mimics the flow of blood in an artery was an involved and complex process. The following section will detail the steps of the process from concept to finished product.

4.1.1 Design Requirements

In the primary stages of designing the pump and artery system, a list of design requirements was generated. The first and most general requirement was to mimic the blood flow curve of the abdominal aorta and iliac arteries. The flow curve, which can be found in Figure 1, depicts the model for replication. In producing the flow curve, it was important that the design capture enough harmonics of the curve to properly interpret any changes in frequency response in a diseased artery.

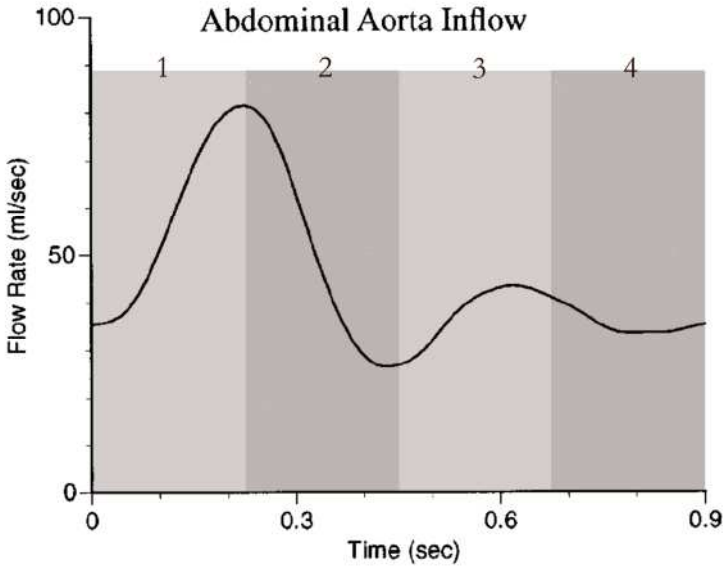

Figure 11: Abdominal aorta flow curve

The second design requirement was the mechanical feasibility of the design. The pump system had to have good manufacturability, be mechanically stable, provide reproducible data, and be cost and time effective. It also needed to work in conjunction with a system to measure flow rates.

4.1.2 Determining an Appropriate Model

Following the development of the design criteria was the model and part selection process. Initial brainstorming was used to develop a list of potential candidates that could fulfill the design requirements. The list was then put through a selection matrix. This matrix, found in Table.1, allowed the potential model to be compared with the needs of the project. Through the selection matrix it was decided to proceed with the cam and piston model for the pump system.

Table 1: Pump model selection matrix

Requirement	**Centrifugal**	**Roller Pump**	**Turkey Baster**	**Cam & Piston**	**Electromagnetic**
Produce Pulsatile Flow	Yes	Yes	Yes	Yes	Yes
Mechanical Stability	Yes	Yes	No	Yes	No
Data Reproducibility	Yes	Yes	No	Yes	Yes
Cost Effective	No	No	Yes	Yes	No
Time Effective	Yes	Yes	Yes	Yes	No

4.2 Design Components

The following section will detail the specific components involved in the production of the cam and piston pump. For each component, the calculations and specifications will be used to explain how the component relates to the overall project.

4.2.1 Designing a Cam

The cam is a device which is capable of generating a repeatable flow curve. In order to design the cam, the flow curve found in Figure 1 had to be digitized. This was necessary to obtain the exact shape of the cam and provide input for the computer. The shape was also dependant upon the stroke length of the attached piston. This shape was developed through the use of Dynacam software, from which a solid model of the part was generated for manufacturing. Each of these components of the cam design will be discussed in more detail in the following sections.

4.2.1.1 Digitizing the Flow Curve

In order to design the cam, it was necessary to obtain a base curve for the cam to mimic. As mentioned previously, Figure 1 depicts a healthy flow of blood through the abdominal aorta. From this flow curve, roughly 170 x and y coordinates were obtained to develop the cam. Digitizing software used to extract points from a scanned curve was not readily available as a resource, so the curve was digitized by hand. Found in Figure 12 is the reproduced flow curve.

After completing the digitizing process, the curve was extended from 50 seconds/cycle to 60seconds/cycle, although the human average is closer to 70 seconds/cycle. This change was made, because a motor was readily available to rotate the cam at this speed and because resting heart beats can vary significantly from one human to another. To do this, the dwell portion of the curve was extended.

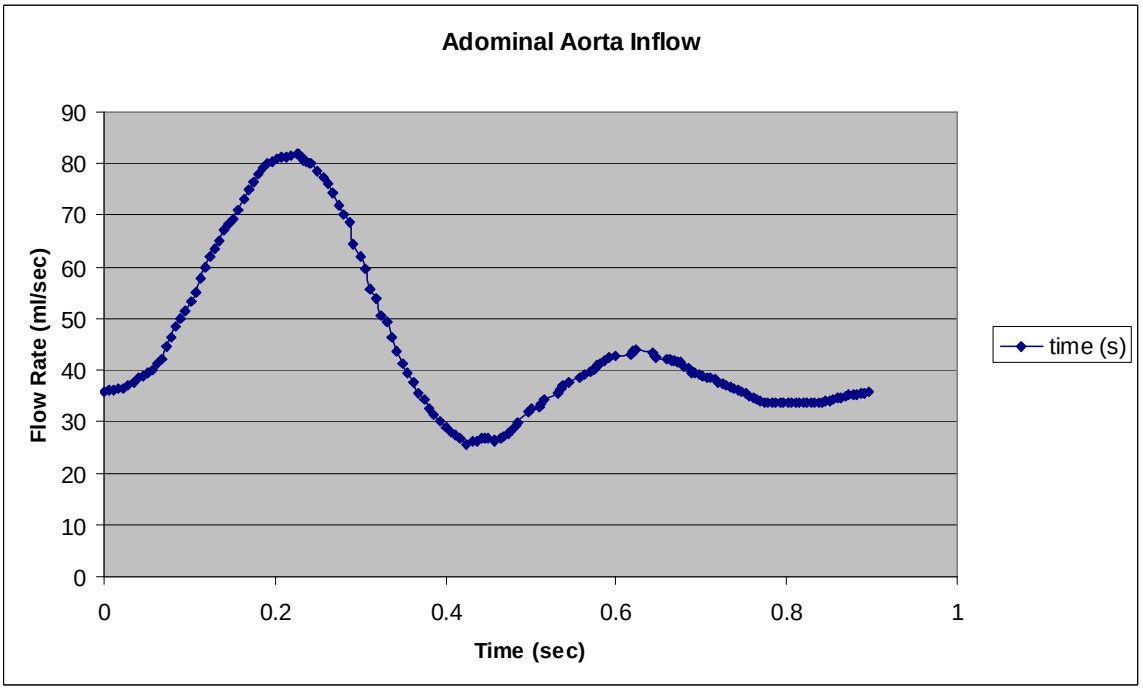

Figure 12: Digitized reproduction of the abdominal aorta inflow curve

4.2.1.2 Calculations for Cam and Piston Stroke Length

The stroke length of the cam and piston section was determined by the piston head size. This piston head size was determined due to constraints in materials. The head

of the piston established the volume of liquid needed to be pushed by each stroke. The larger the head the shorter the stroke needed. In addition to the stroke calculations, the location of the high and low points of the flow curve had to be determined in relation to the 360° rotation of the cam. The calculations below represent the various trials and designs that were done in order to find the ideal cam. In the calculations below the diameter was determined and from this diameter, the stroke was determined. The stroke was calculated by determining the maximum length of the cylindrical volume of liquid that is needed to be pumped. After this length was determined it was necessary to determine the degree locations of the maximum stroke, the minimum stroke and the peak of the second section of the wave. This was done through a simple ratio. Calculations were done to determine exactly how long the stroke had to be to propel the correct amount of fluid through the system. This ratio was based on the diameter of the piston head and the length the cam had to propel the piston. The following design calculations were done based on the size of piston head. These three designs were done with increasing piston head size. It was found that with a larger piston head the cam design had less jerk and provided a much smoother design. This smoother design allows for the follower system to remain flush with the cam and completely mimic the desired curve.

1st Cam Design

D=20mm

R= 10mm

Volume= $\pi * r^2 *$ maximum Stroke length

$56250mm^3 = \pi * (10mm)^2 * L$

L= 179mm

$$\frac{360 Degrees}{1.000531 \sec} = \frac{X}{0.254742 \sec} \quad \leftarrow 179 \text{ mm}$$

X= 91.7°

$$\frac{360 Degrees}{1.000531 \sec} = \frac{X}{0.474847 \sec} \quad \leftarrow 0\text{mm}$$

X= 170.9°

$$\frac{360 Degrees}{1.000531 \sec} = \frac{X}{0.69607 \sec} \quad \leftarrow 58.1\text{mm}$$

X= 250.5°

2nd Cam Design

D=1.375 =3.4925cm = 34.925mm

R= 17.5mm

$56250\text{mm}^3 = \pi * (17.4625\text{mm})^2 * H$

H= 58.8mm

$$\frac{360 Degrees}{1.000531 \sec} = \frac{X}{0.254742 \sec} \quad \leftarrow 58.7\text{ mm}$$

X= 91.7°

$$\frac{360 Degrees}{1.000531 \sec} = \frac{X}{0.474847 \sec} \quad \leftarrow 0\text{mm}$$

X= 170.9°

$$\frac{360 Degrees}{1.000531 \sec} = \frac{X}{0.69607 \sec} \quad \leftarrow 19.05\text{mm}$$

X= 250.5°

Final Cam Design

D=1.1875 =3.01625 cm = 30.1625mm

R= 15.1mm

$56250mm^3 = \pi * (15.08125mm)^2 * H$

H= 78.7mm

$$\frac{360 Degrees}{1.000531 \sec} = \frac{X}{0.254742 \sec} \quad \leftarrow 78.7 \text{ mm}$$

X= 91.7°

$$\frac{360 Degrees}{1.000531 \sec} = \frac{X}{0.474847 \sec} \quad \leftarrow 0mm$$

X= 170.9°

$$\frac{360 Degrees}{1.000531 \sec} = \frac{X}{0.69607 \sec} \quad \leftarrow 25.5mm$$

X= 250.5°

4.2.1.3 Dynacam

Designing the cam was crucial to the final design. A reliable method of cam design is the computer program Dynacam, developed by Professor Norton of Worcester Polytechnic Institute. Through meetings with Professor Norton and knowledgeable users of the program, a proper design for the cam was produced. The cam was based off a

single spline curve. Figure 13 shows where the numbers calculated above were inputted into the program.

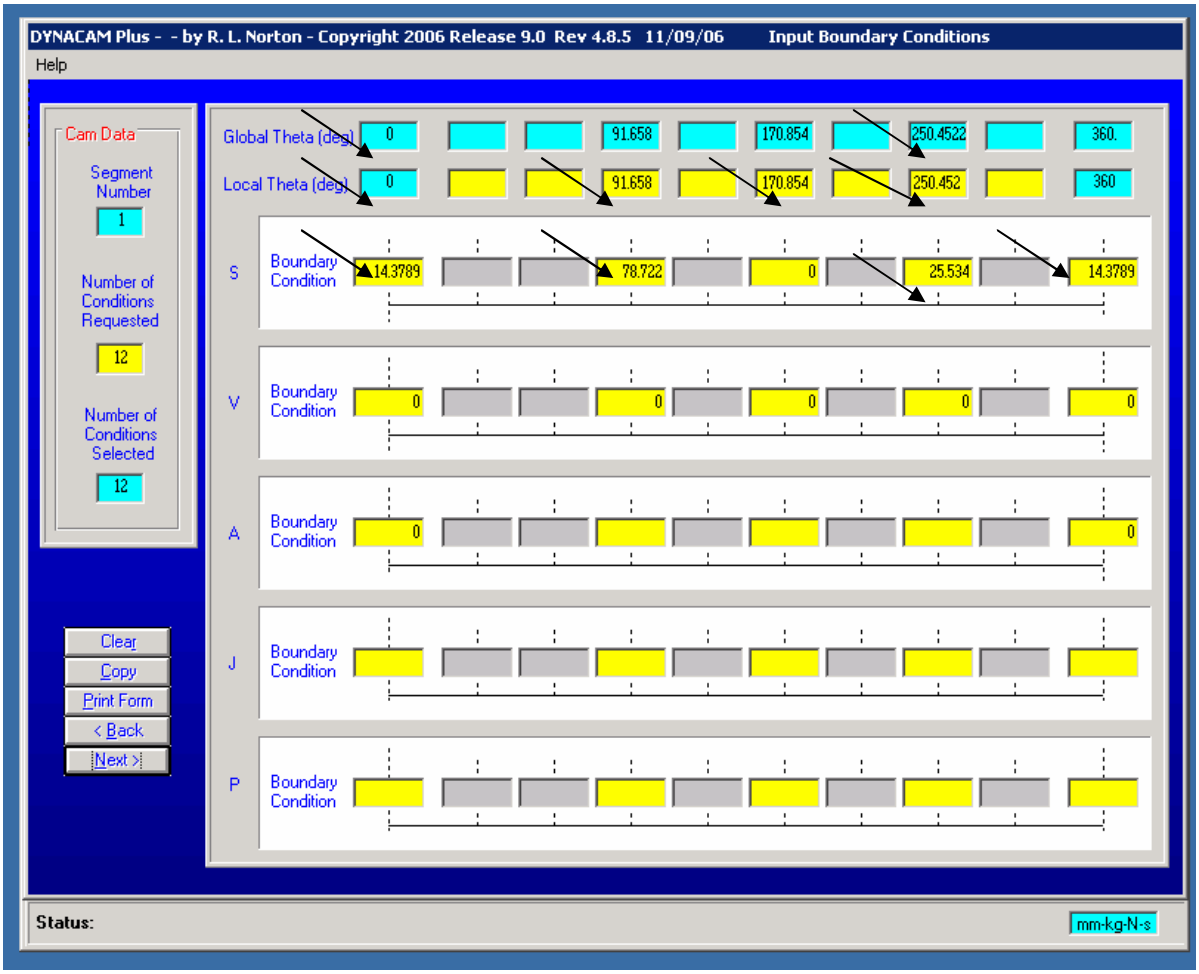

Figure 13: Dynacam value input screen

Figure 13 shows how the cam was developed using 12 constraints. Values were inputted for the start and finish, the peaks of the first and second parts of the wave, and the lowest point on the wave. These were the points calculated through our ratio. The other constraints where the locations where the velocity equals zero, which is where velocity is known. The spline order was then determined using these values, as shown in Figure 14. From Figure 4 it is clearly apparent that the Dynacam spline curve closely resembles the flow curve found in the literature. After the development of the spline curve, the cam was

sized and drawn in Dynacam.

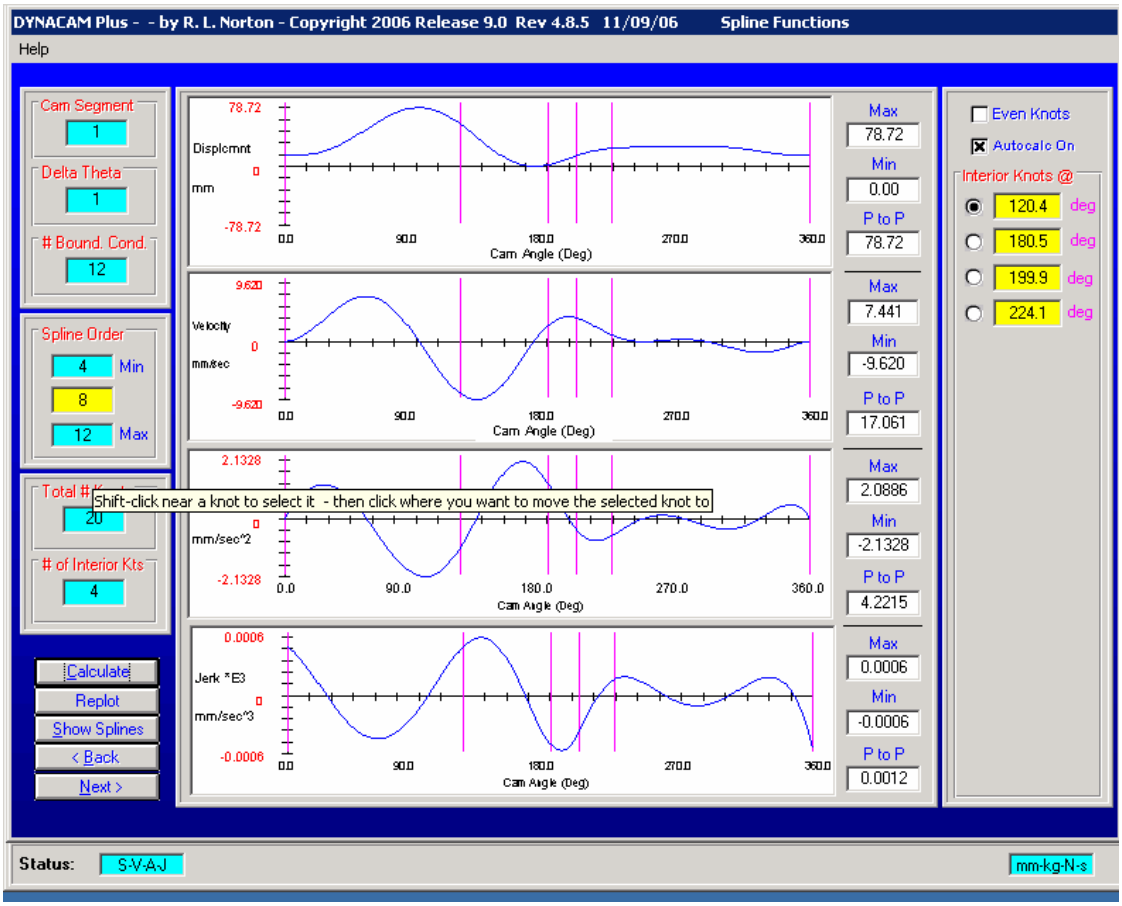

Figure 14: Dynacam plot

A primer radius of 120mm and a roller radius of 20mm were chosen to yield the best results during simulation tests. These values gave an ideal maximum and minimum pressure angle with the smallest primer radius. The final drawing of the cam made by the Dynacam program can be seen in Figure 15. Information from this program was then exported to a solid modeling program to allow for machining.

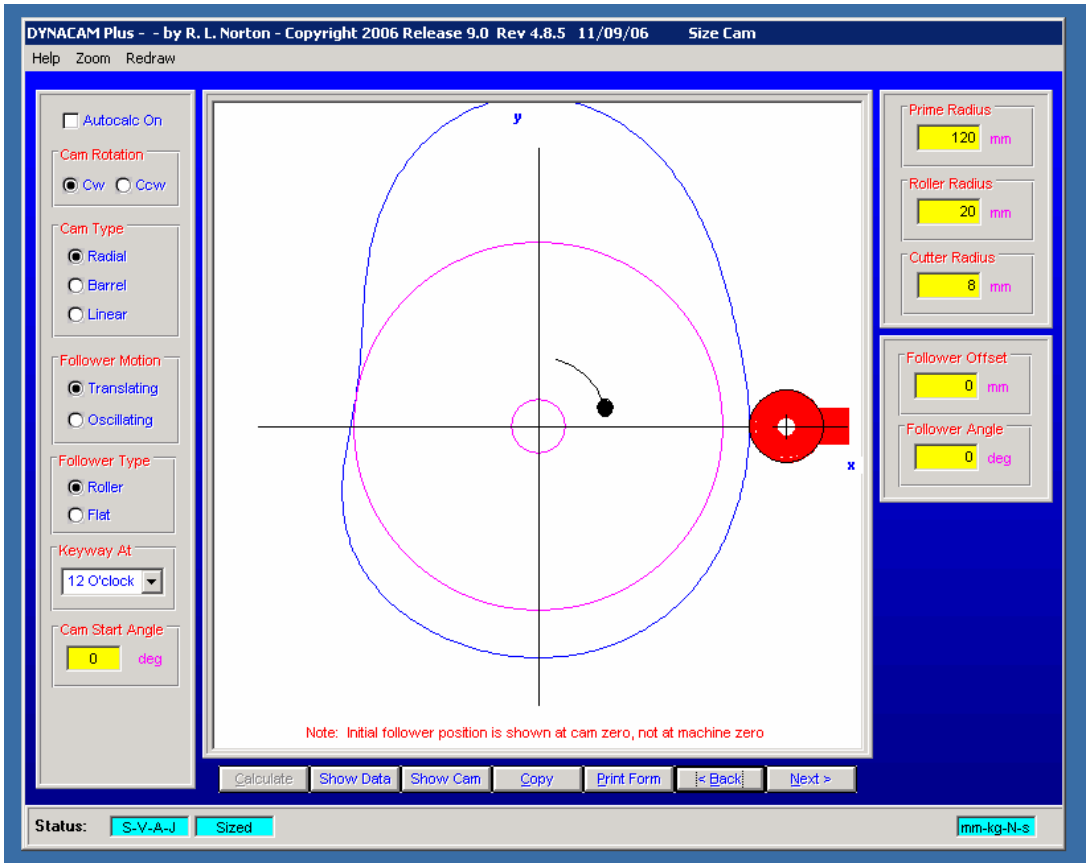

Figure 15: Dynacam drawing of finalized cam shape

4.2.1.4 Computer Aided Design

Solidworks was used to import and model the cam design. A solid model of the cam design was developed to allow for machining. In order to do this the x and y coordinates were exported from Dynacam into a Microsoft Excel spreadsheet. The solid model was based off the spline curve developed from the x and y coordinates exported from Dynacam. In order to draw this spline curve correctly it was necessary to select the spline curve through 'xyz' in the Solidworks menu. The Excel spreadsheet was resaved as a CSV (Comma delimited) (*.csv) file which was used to import the points into Solidworks. An ungrounded spline curve was then drawn through all the points in the excel file. In order to ground the sketch, the offset button was pressed. The sketch was grounded by using the offset button and was extruded into the part to be machined.

4.2.2 Designing the Piston and Follower System

The cam was designed from measurements of the piston head. The actual outside diameter used for the measurements was the size of the o-ring fitted to the piston. The o-ring had an outer diameter of 1-and-3/16 inches; therefore the rest of the piston follower system had to be made based on the dimensions from that measurement. Just as the stroke length played a part in designing the cam, it also influenced the design and dimensioning of the piston and follower system.

4.2.2.1 The Piston

The piston head is the most important piece of the system because it is the only piece in contact with the fluid being pumped. There are many subtleties to the piston head's function, because not only does the structure of the head need to be sound, but it must provide a proper area for the o-ring to completely block any backflow of the fluid. If the o-ring does not fit in the piston well or fully block the fluid from flowing backwards, the flow curve will not match the flow found in a human abdominal aorta. The piston head was constructed out of aluminum and consists of a cylinder with an indented ring near the top of the piston to host the o-ring, and a threaded hole on the opposite side through the center. The hole has a depth of two inches, a diameter of two-and-a-half inches, and eight threads per inch. The computer aided design program used to generate the machine drawings was ProEngineer. The ProEngineer drawing of the piston head can be seen below in Figure 16.

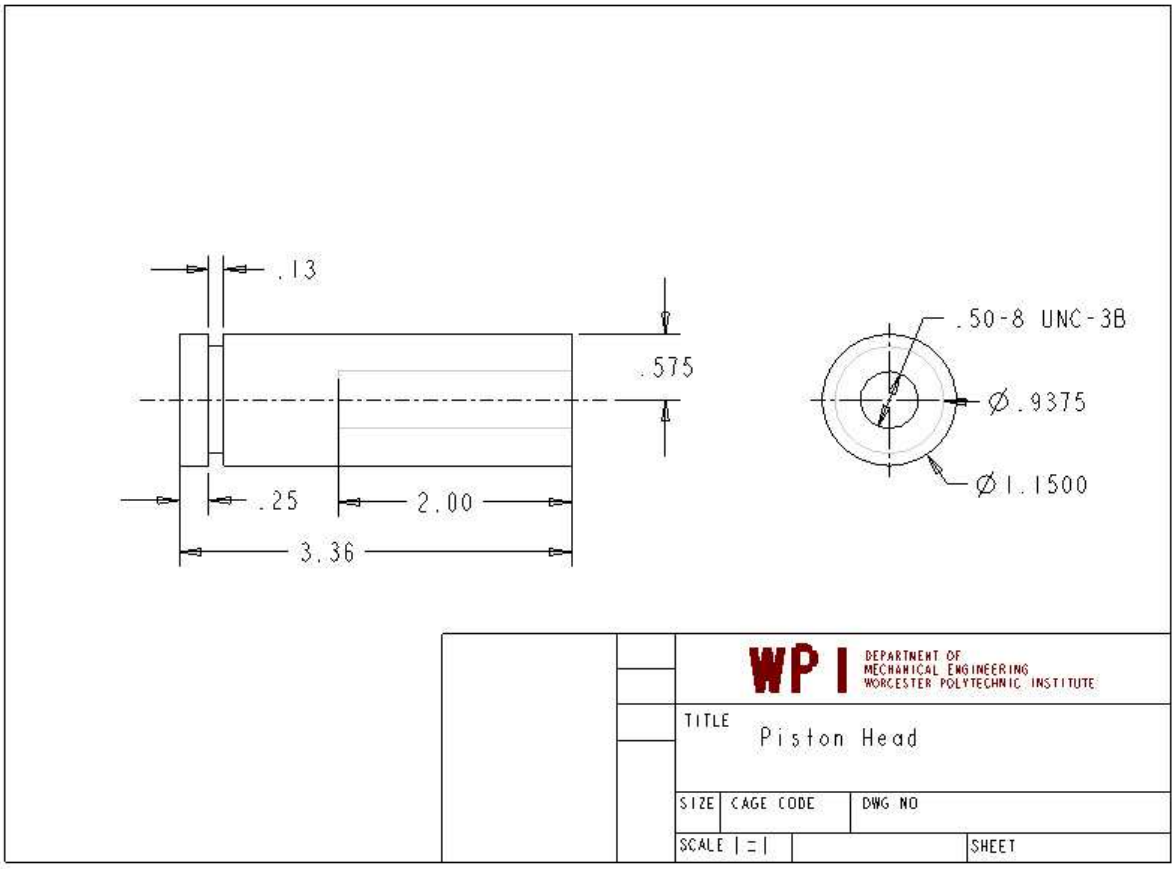

Figure 16: Drawing of the piston head created using Pro Engineer

4.2.2.2 The O-Ring

The O-ring is the part that prevents any backflow by providing a watertight seal between piston and tube. Physically it rests in the indent of the piston and its dimensions are an outside diameter of 1 and 3/16 inches, an inside diameter of 15/16 inches, and width diameter of 1/8 inches. The o-ring used in this product was produced by Danco, Inc..

4.2.2.3 The Piston Shaft

The shaft, along with the piston head and follower make up the main component of the pulsatile flow device. The shaft connects the piston head to the follower by means of two threaded ends that correspond to the threaded holes of the two pieces. It is uniform in diameter except for an extended portion that is involved in the mechanism needed to apply constant pressure towards the cam. The area is 1.5 inches, and protrudes 1.5 inches in diameter beyond the normal 0.5 inch diameter shaft. The ProEngineer drawing of this part can be seen in Figure 17.

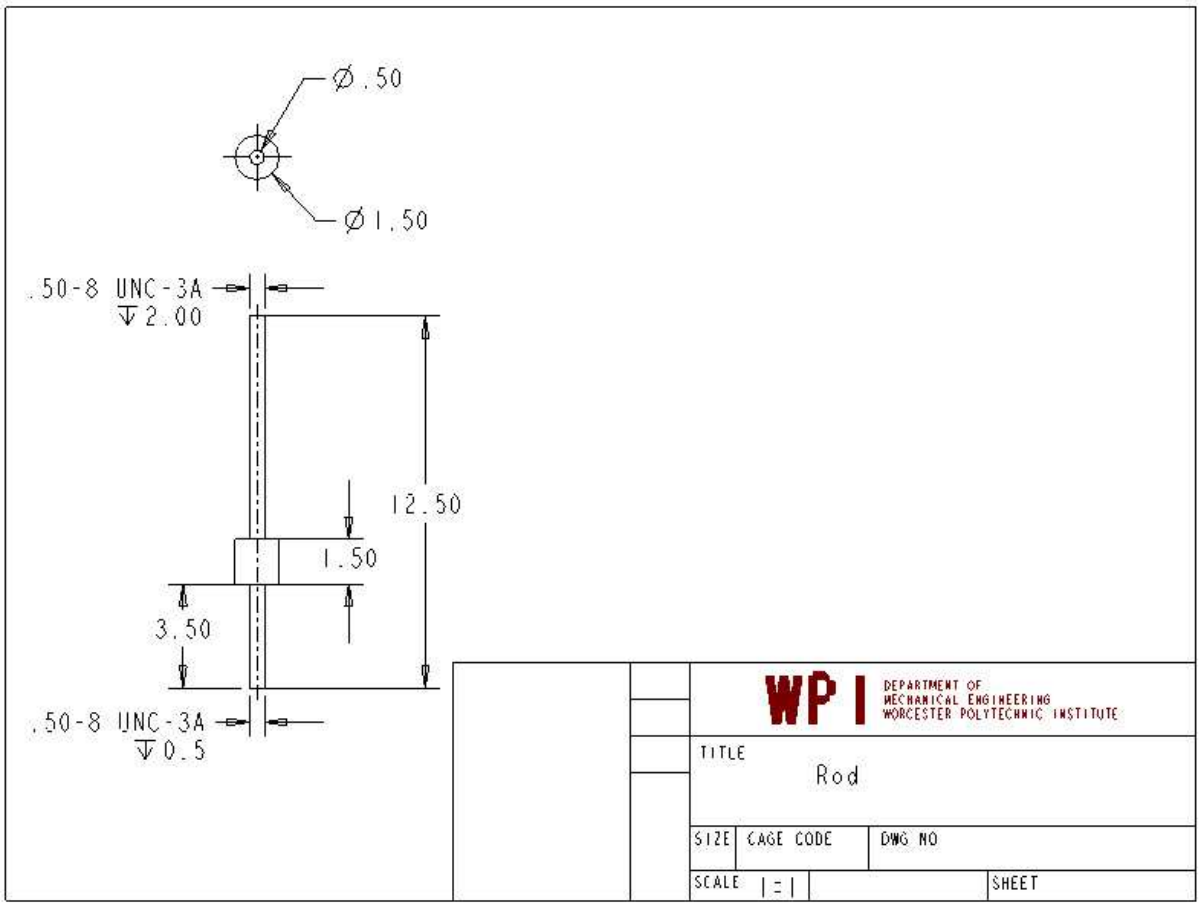

Figure 17: Drawing of the shaft created using Pro Engineer

4.2.2.4 The Spring

In addition to the extended portion of the shaft, a spring applies force from the piston back on the cam. The part ensures that all the motions of the cam are captured in the stroke. The spring is placed around the shaft with one end pressed against the enlarged diameter of the shaft with the opposite end will flush against the first support structure of the artery setup in order to keep a constant force on the shaft itself towards the cam. Without this spring force the piston head would never pull back in accordance with the pressure curve and the machine would only be capable of pumping the fluid once.

4.2.2.5 The Follower

The follower is located at the end of the shaft opposite the piston head and is the connection of the rest of the system to the cam. It is constructed out of aluminum and

consists of a rod that has a threaded hole on one end into which the shaft is screwed. The other end of the rod branches into two sides with two 1/4 inch holes located in the middle of each of them. These side supports hold bumpers to travel along the cam. This will provide constant force on the cam and the piston head will move in accordance to the movement of the cam itself. The ProEngineer drawing of this part can be seen in Figure 18.

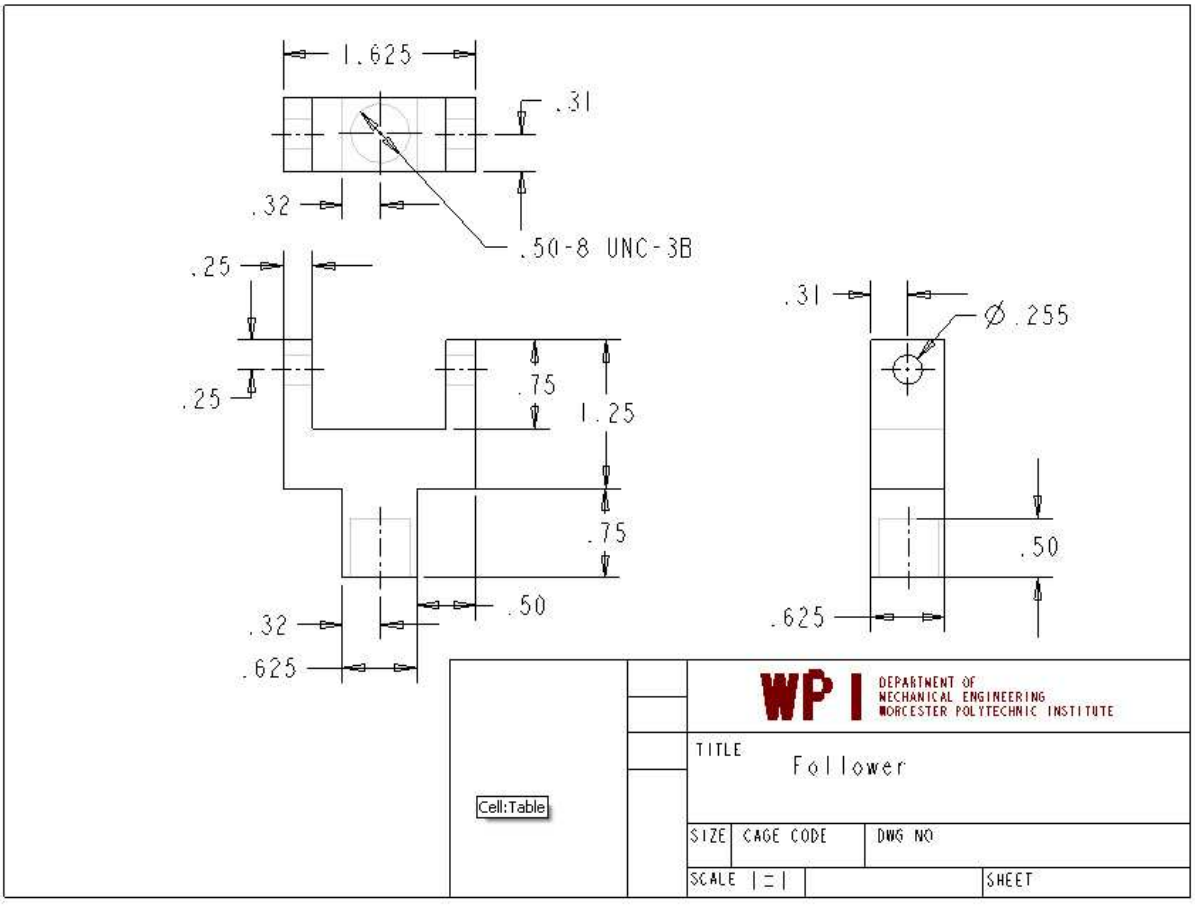

Figure 18: Drawing of the follower created using Pro Engineer

4.2.2.6 Axle

The axel interlocks with the cam and will be placed through the end of the follower. It is attached by a grooved wheel will say in place through the hold of two nuts. The two nuts are 1/4 inch in diameter and have 22 threads per inch. They will both be placed at the ends of the axel to keep the follower and in one solid piece. The drawing of this part can be seen in Figure 19.

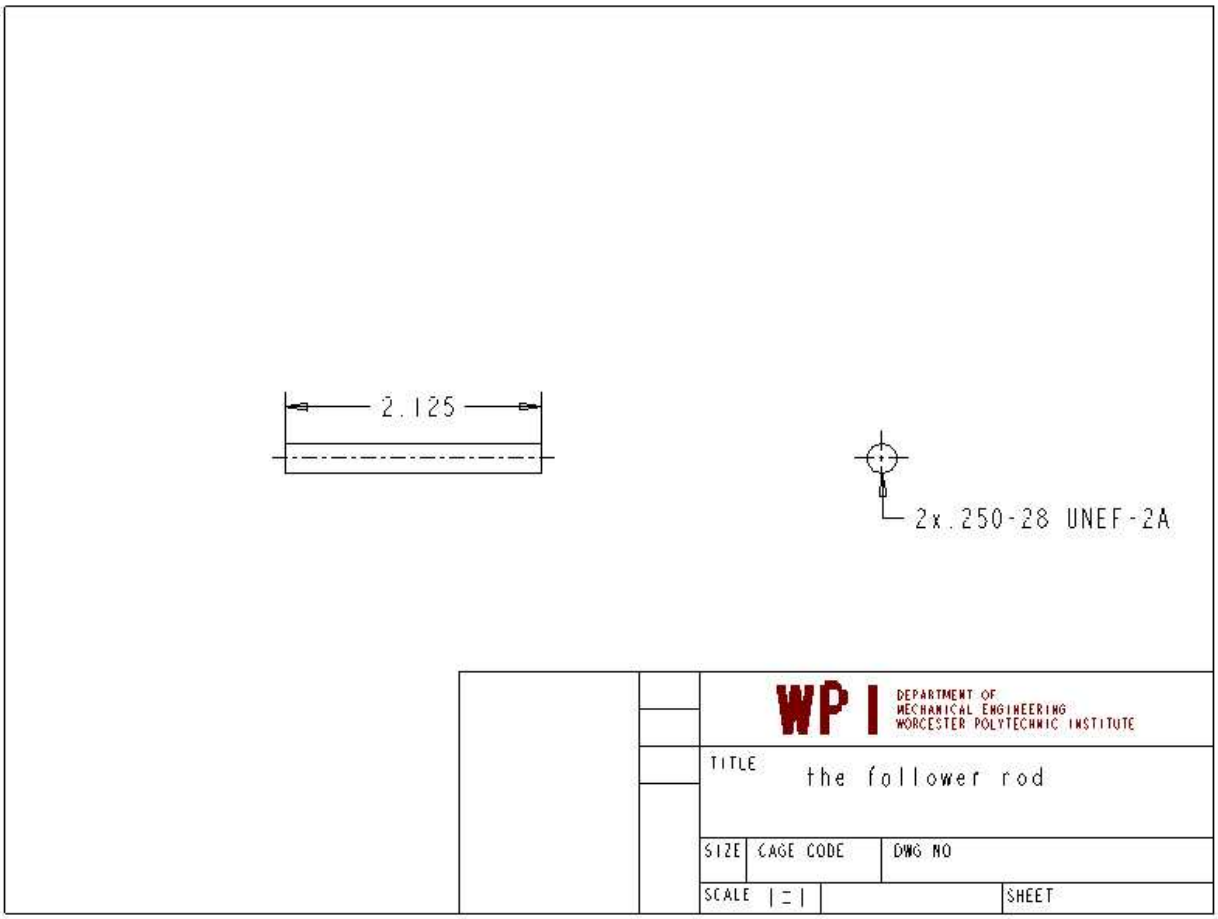

Figure 19: Drawing of the axel of the follower in contact with the cam created using Pro Engineer

4.2.2.7 Supports

The two supports are extremely similar in structure, the only differences being the size of the holes through each. The second support has a larger hole than the first because of the enlarged area on the shaft that will be passing through it. The reasoning is that the spring needs to be fixed on the end which will be the first support. Here the hole is just large enough for the smaller diameter to slide through. The other end, however, allows the shaft to slide back and forth through the second support providing the necessary force against the cam. The drawing of these parts can be seen in Figures 20 and 21.

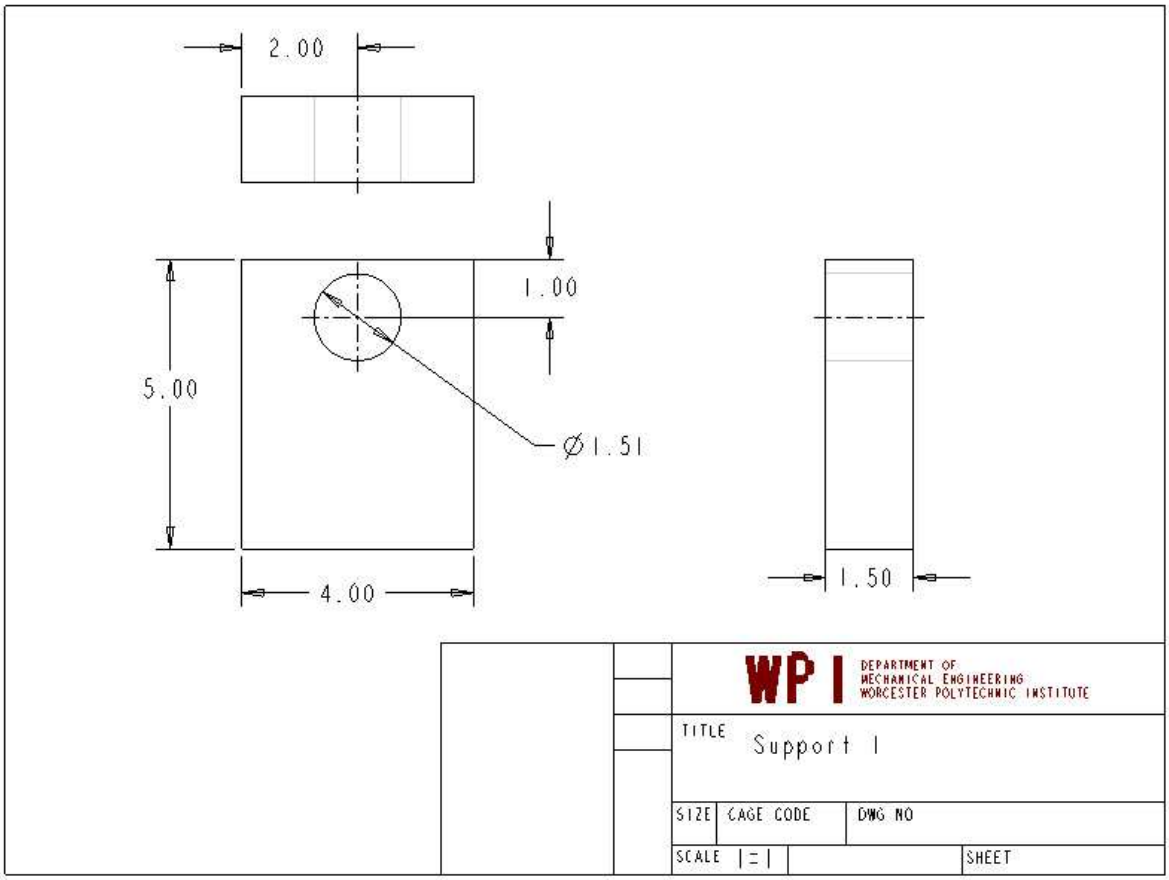

Figure 20: Drawing of the support closest to the follower created using Pro Engineer

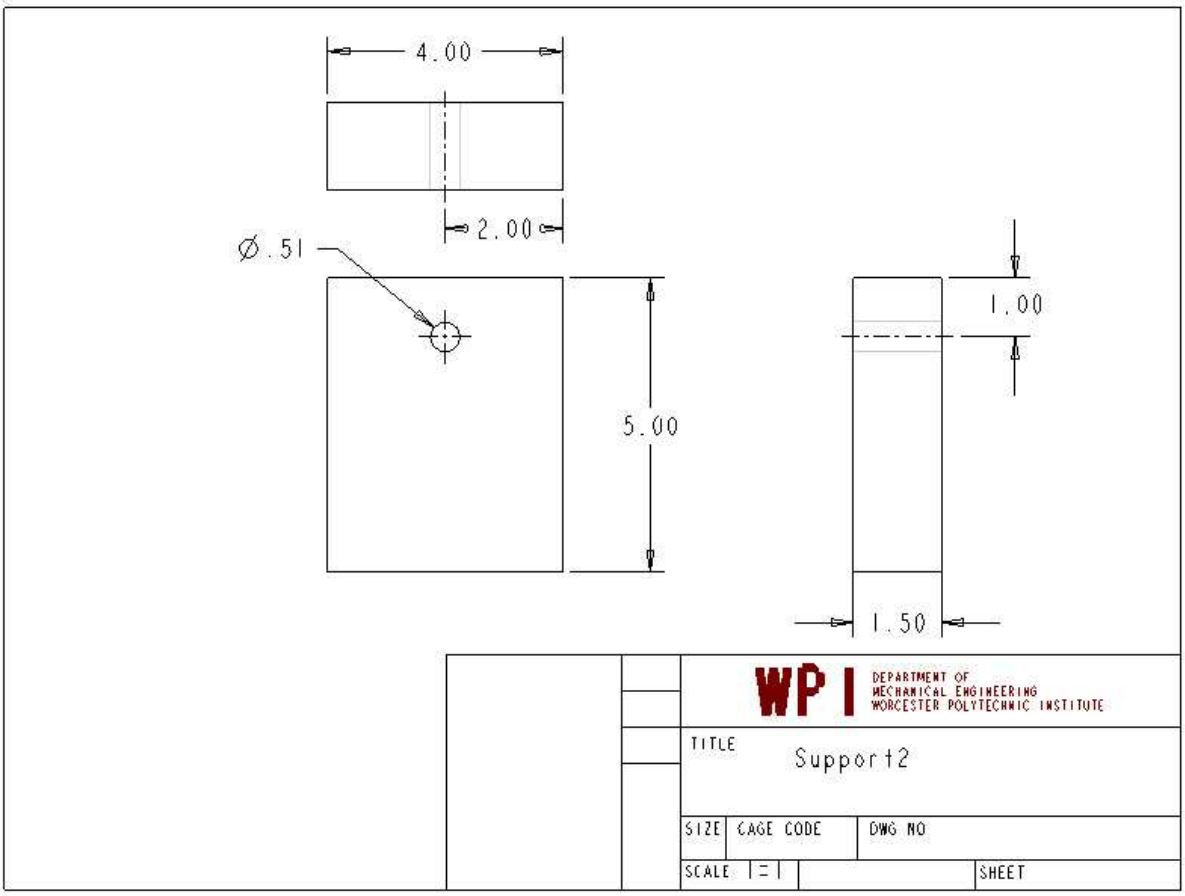

Figure 21: Drawing of the support closest to the piston head created using Pro Engineer

4.2.2.8 Piston Housing

The piston housing is the part in which the piston contacts the fluid. The housing is made from a plastic tube, unlike all the rest of the pieces composed of aluminum. The plastic is clear so any potential flow problems can be observed. From this housing, the fluid is pumped into the arterial setup. It is the transition area from the system itself to the articles that are being tested.

4.2.3 Selecting an Appropriate Test Material

In the development of our heart pump and artery system, a suitable material to mimic the properties of the arteries had to be found. Various calculations were made to determine which material would best mimic an artery wall, and the sizes we would need for the two arteries. The following section details the material selection process.

4.2.3.1 Physical Properties.

Through literature searches, the physical properties of the arteries to be recreated in the experiment were collected. The summary of radii, wall thickness and elastic modulus of both the iliac and abdominal aorta can be found in Table 2. The values in the table provided enough information to perform the calculations necessary to determine what type of tubing was feasible. The radii and thicknesses are given as ranges, because these are the average values for human abdominal and iliac arteries. Since no two individuals are the same, there is not a universal value for either of these.

Table 2: Ranges of values for the radius, thickness, and elastic modulus of the abdominal and iliac arteries

	Abdominal artery	**Common iliac artery**
Radius (R)	0.548 - 0.610 cm	0.350 - 0.368 cm
Thickness (t)	0.078 - 0.084 cm	0.06 - 0.063 cm
Elastic Modulus (E)	4×10^6 dyne/cm^2	4×10^6 dyne/cm^2

Based on the values found for the abdominal and iliac arteries, common piping or tubing materials was researched. The elastic moduli (E) of the arteries are very low compared to that of most tubing, so the research focused on tubing with a low E. Since the main focus was on wall motion, compliance was more important than just E. By not scaling our model, the compliance calculations allowed for a little flexibility in at least 2 of the variables. The elastic modulus of any feasible material cannot be changed, but the radius and thickness can. Table 3 below lists the E values found for various tubing materials.

Table 3: Elastic modulus values of typical tubing materials

Material	**Elastic Modulus (E) (dyne/cm^2)**
PE	$5 \times 10^9 – 12 \times 10^9$
Low density PE	2×10^9
Rubber	1×10^8

4.2.3.2 Compliance Calculations

To determine whether the tubing could serve as an accurate representation of an abdominal or iliac artery, the compliance of each artery was calculated using the equation:

$$C_r = \frac{R^2}{Et}$$

In the above equation, Cr is compliance, R is the radius of the tubing, E is the elastic modulus of the material, and t is the thickness of the tubing. Since each variable in the equation, with the exception of E, was given a range of values, the compliance was also calculated as a range. The compliance of each artery was found to have a high and a low value, denoted as a small H or L, respectively, as shown in Table 4 below.

Table 4: High and low compliance values for the abdominal and illiac arteries in the average human

Compliance	**Abdominal Artery**	**Iliac Arteries**
C_H	1.19×10^{-6} cm^3/dyne	8.938×10^{-7} cm^3/dyne
C_L	5.64×10^{-7} cm^3/dyne	4.86×10^{-7} cm^3/dyne

Using the compliance values calculated for the abdominal artery, equation 1was rearranged to solve for the tube thickness:

$$t = \frac{R^2}{EC_r}$$

Using the original radii values from Table 2, the E values found in Table 3, and the compliance values found in Table 4, a range of thicknesses for each material listed in Table 3 were calculated. As shown in Table 5 below, the results yielded no feasible thicknesses.

Table 5: High and low values for the thickness of various tubing materials

Material	$\mathbf{t_H}$	$\mathbf{t_L}$
PE	8.3266×10^{-5} cm	2.0938×10^{-5} cm
Low density PE	2.0817×10^{-4} cm	1.259×10^{-4} cm
Rubber	0.0416 cm	0.02518

Based on the extremely small numbers calculated for the thicknesses, it was acknowledged that changing the radii values by a small amount would be of no help in this matter; however the rubber thicknesses came out to be considerably close to an obtainable thickness. This led to more research on other possible tubing materials. A ductile tubing material, Penrose tubing, was found, with an elastic modulus of 6.07×10^7

dyne/cm2 and a measured thickness of 0.02 cm.. Various radii were available for order, so the former compliance calculation was rearranged again to solve for the radius:

$$R^2 = C_r E t$$

After substituting the compliance of the abdominal aorta and the E and thickness of the penrose tubing, the calculated radius was 1.2 cm. Converted to inches, it was found that the necessary radius was 0.47 in. Since the values for the abdominal aorta vary from individual to individual, 1 inch diameter Penrose tubing was ordered for the abdominal aorta. Actual values can be seen in table 6.

Table 6: Compliance calculation values

	Abdominal Aorta	**Abdominal Penrose**	**Iliac Arteries**	**Iliac Penrose**
C_R (calculated compliance) [cm^3/dyne]	9.6×10^{-7} - 1.19×10^{-6}	1.33×10^{-6}	3.64×10^{-7} - 4.3×10^{-7}	3.3×10^{-7}
E (Young's Modulus) [dyne/cm^2]	4×10^6	6.07×10^7	4×10^6	6.07×10^7
t (thickness) [cm]	0.078 - 0.084	0.02	0.078 - 0.084	0.02
R (radius) [cm]	0.548 - 0.61	1.27	0.35 - 0.368	0.635

Similar calculations were performed to determine that the Penrose would also work for the iliac arteries. Based on the compliance values found for the iliac arteries, listed in Table 4, and the known values for thickness and E of penrose tubing, the calculated ideal radius of the tubing would be equal to 0.3024 inches. Similar to the justifications for the abdominal aorta, it was decided to order tubing of 0.5 inch diameter.

4.3 Obtaining Data

4.3.1 Pressure Transducers

Pressure transducers were selected to measure the pressure changes within the simulated arteries and retrieve the data necessary for analysis. The transducers were inserted into the arterial tubing towards the ends of the simulated iliac arteries. The transducers themselves were amplified output transducers for 5Vdc power. The Omega PX139-030D4V transducer was chosen for its 0-30psi measurement range. Additional product specifications are listed below in Table 7.

Table 7: Information for the pressure transducers

Excitation Voltage	5 Vdc @ 2mA
Output	0.25 to 4.25 Vdc
Span	4 V +/- .1 V
Repeatability	+/- 0.3%FS

4.4 Viscosity Calculations

The system developed to mimic blood flow in the abdominal and iliac arteries was created with a 1 to 1 scale. This required the use of a fluid other than water to match the viscosity of blood in our system. In order to correctly determine the viscosity of the sugar water, we developed a capillary viscometer to ensure that the viscosity of water could be correctly calculated. Water was poured into a container, which had a small tube attached to the bottom. A known volume of water was timed flowing out of the tube at the bottom. Using the following equation we were able to verify that the viscosity of water was 1 cP:

$$\Delta P = \frac{128 \mu Q L}{\Pi D^4}$$

In this equation, the change in pressure was calculated by multiplying the density of water by gravity and the length of the tube it flowed out of. Q was the flow rate, as determined by the amount of time the known quantity took to come out of the tube. L was the length of the tube, and D was the diameter of the tube. Solving for viscosity, a value of 0.97 cP was found for water. This allowed for calculations for the sugar water.

A 25% sugar water solution was used in the same experiment mentioned above. The same calculations were performed to obtain a value of 3.0 cP. A 50% sugar water solution was also in the same experiment and the same calculations were done. The viscosity of the 50% sugar water was found to be 3.8 cP. Using the viscosities of water and the two sugar waters, we interpolated and estimated that a 40% sugar water solution would best mimic the viscosity of blood. After running an experiment with the 40% sugar water in the capillary viscometer, and using the equation above, the viscosity was found to be 3.21 cP with a Reynolds number of 23 and Womersley number of 5.76 . The

average viscosity of blood is found to be between 3.2 and 3.5 cP, allowing for the 40% sugar water solution to be used as a suitable blood substitute.

4.5 Assembly of Device

The device was designed to be a volumetric pump that was driven by a cam attached to a motor. The system was developed to convert the rotational motion of the cam to linear motion of the piston. This complete system was complex with ten parts, consisting of eight moving parts and two stabilizing parts. This system started off with the custom designed cam which was attached to the motor. The particular motor had a maximum speed of 120 RPM which was well above the necessary speeds. This motor was powered by a STACO EJ90LV isolated AC/DC power supply. This motor powered the cam at the appropriate speed causing the piston head to move according the custom contours of the cam.

Seen in figure 22 is the piston and support system consisting of intricate parts that are all necessary to propel the fluid through the system. First the system starts with a yoke piece that included a pin which provided the contact point for the cam. In order to reduce friction and wear between the cam and piston a lubricated bearing was placed around the pin that allowed for reduced friction while still providing the correct constant motion. This yoke system was pressed on to the main rod. A large cylinder was placed around this main rod to increase the diameter of the rod for a particular segment. This increase in diameter is necessary for the correct function of our support system. At the end of the rod our piston head was pressed on and the commercial o-ring was slipped into the custom made groove. This piston system was threaded into our two supports as seen in figure 22.

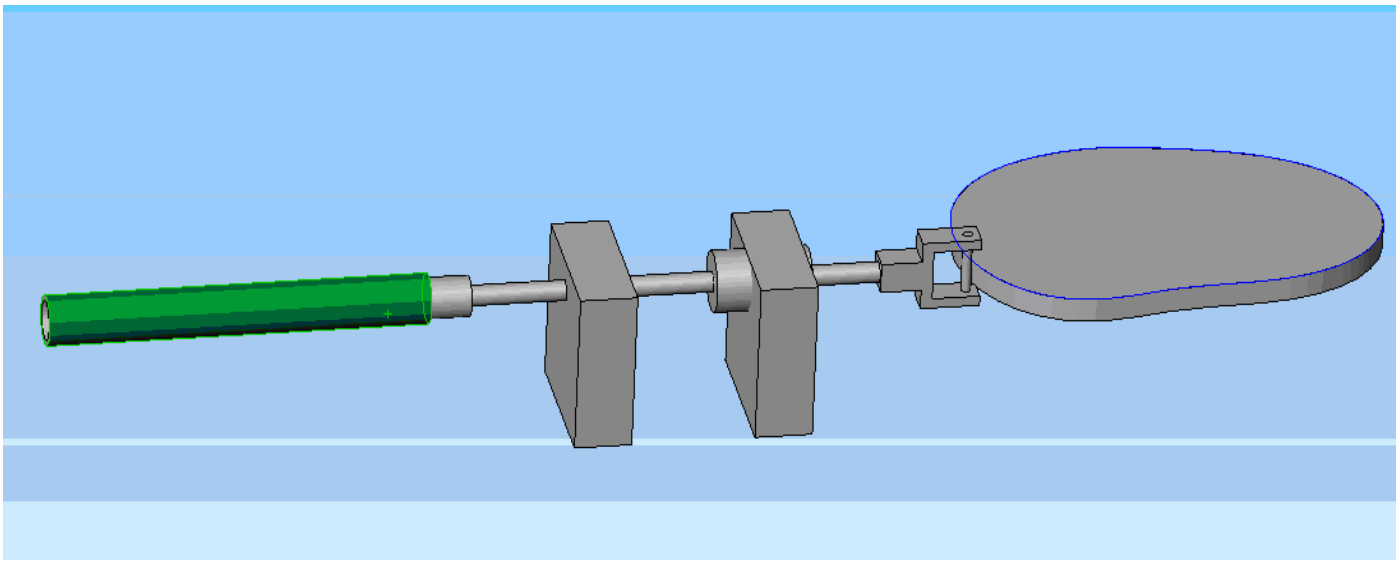

Figure 22: Assembly drawing

Also two springs were threaded around the piston rod between the larger diameter and the support with the smaller diameter. These springs provides the system with the constant recoil pressure that was necessary to keep the bearing flush against the cam through its full rotation. These supports provided the necessary structured base needed for the springs to provide the necessary recoil, while also providing stabilization for the entire system. These two supports also keep the system stable and remove the risk of lateral motion during the linear motion of the piston.

This entire piston system is attached to a two layer wooden base which contains five legs supports. The motor itself is dropped into the top layer through a custom cut hole and bolted down to increase its stability. These two supports were also bolted down to the top layer of the base which allows for optimal stability.

The loading section of the system was a clear plastic tubing cut to size. This tubing acted as the location where the fluid would fill and then be propelled by the piston. The fluid is fed through a tubing system using gravity as the driving force. The reservoir is located at an elevated height with a quarter inch tubing that is connected through super glue. This tubing was connected to a ball valve which controled the flow of the fluid from the reservoir into the system. This valve was connected to another tubing set which was connected to a check valve. All connections between the tubing had been clamped down to remove the risk of leakage. This check valve was connected to the loading chamber

through super glue and stay put plumber's putty. This entire feeding system was water proof and supplied the entire system with the fluid. The check valve connected the water feeding system with the loading chamber.

The loading chamber was clamped down to two wooden supports, which stabilized the system through the motion of the piston, while also setting it at the appropriate height. The test piece, the penrose drain, was connected to the loading piece through another clamp. The test piece was placed on its support stand which consisted of a wooden block stand with a Plexiglas top. This test piece was kept in place with a set of three clamps which allowed for slight movement while also stabilizing the penrose drain.

Each iliac branch was connected to a small diameter tubing which fed the fluid from the system into a collecting basin. These two tubes were also connected to the penrose drain through two clamps. These clamps provide the system with the vascular resistance similar to that found in the body. The last part of the system was the location of the pressure transducers. These two transducers are located at the inlet and outlet of the system. In order to get a correct reading the transducers were mounted above the penrose test piece. To mount the transducers, a wooden platform was assembled and they were bolted into the front and back to accommodate readings from both the inlet and outlet.

4.6 Running of the system

In order to run the system the power supply was set to 2.5 volts which allowed for the cam to rotate at 60 rpm. The ball valve was then opened to release the fluid into the system. The piston follower system followed the contours of the cam staying flush as a result of the spring recoil. The piston then pushed the fluid through the loading system into the penrose test piece. Then the pressure was read by the transducers and the waveform was outputted into the labview program. The labview program exported the data to Microsoft excel where it can properly analyzed.

4.7 Artery Systems and Blockages

4.7.1 Artery System

The artificial artery systems were constructed with ½" diameter and ¼" diameter Penrose tubing. Each system consisted of one ½ " tube cut to 15cm in length, and 2, ¼ " tubes cut to 7cm in length. These values were obtained from normal physiological conditions referenced in the literature review portion of this paper. An additional length was allowed when cutting the tubing to allow for overlap when connecting the system to the mechanical pump.

Loctite medical adhesive was used to attach the abdominal aortic section to both iliac models. The adhesive was delivered through a small diameter applicator tip to ensure a thin application. Care was taken to guarantee the adhesive adhered to all areas where the abdominal aorta and iliac arteries overlapped.

The Loctite medical adhesive was used for its non-reactive nature and ability to hold a water tight seal. Additionally, its rapid set technology allow for precision and immediate results. Seen below in Figure 23 is the finished artery system. The system pictured did not contain any blockages and was used as the control.

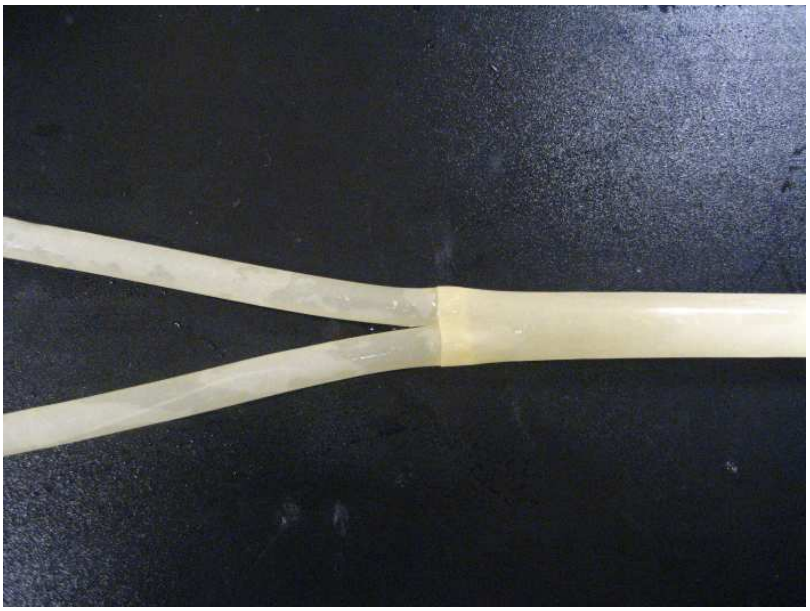

Figure 23: Control artery system, no blockages

The pressure transducers necessary for the data acquisition portion of the project required a physical attachment to the artery systems. Small holes were made with scissors into the completed artery systems at the inflow of the abdominal aorta and exit of 1 iliac artery. Flexible plastic tubing was placed in the holes and secured by Loctite adhesive to ensure a watertight seal. The transducer lead tubing was placed flush with the Penrose so as not to create any disturbance or additional turbulence to the flow.

4.7.2 Arterial Blockages

The arterial blockages were created in a range of sizes. Literature was used to determine the following criteria:

Table 8: Criteria for arterial blockage size

Size	% of Cross Sectional Area (Iliac)
Minimal	10-15
Medium	30-50
Large	75-90

The blockages themselves were created using a heated, rapid cooling, non-reactive glue. When hardened, the glue maintained a tackiness and rigidity similar to blockages found in the targeted diseased conditions. The blockages were placed in physiologically relevant positions in the iliac arteries based on literature, 1-2cm down the iliac arteries from the abdominal aorta split. Additionally, in compliance with the actual diseased state, the occlusions were not made uniformly around the artery, but off center as seen in Figure 24 below.

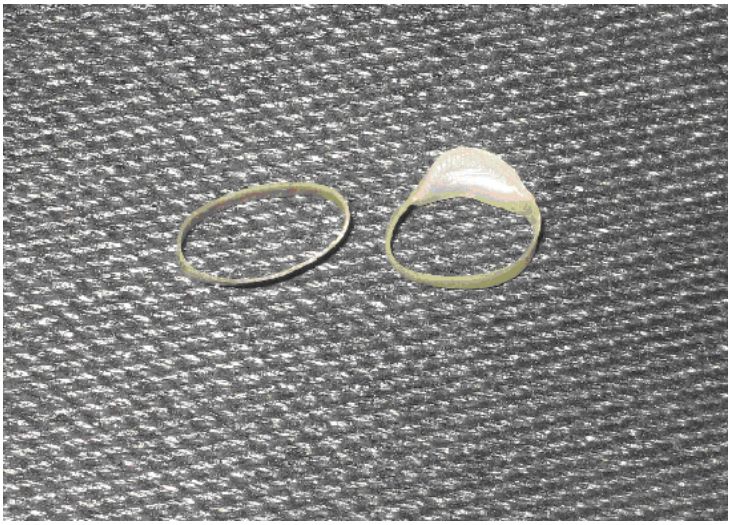

Figure 24: Image of control artery and arterial test blockage in illiac

Test articles were made in the following proportions:

Table 9: Summary of test articles and placement of blockages

Size	Iliac Placement	Number of Samples
No Blockage/Negative Control	N/A	3
Minimal	Right Iliac	3
Minimal	Both Iliacs	3
Medium	Right Iliac	3
Medium	Both Iliacs	3
Large	Both Iliacs	3

Test systems were made with blockages in both arteries to examine the effect double blocked arteries as compared to single blocked arteries. Additionally, it was determined that it would not be common in normal physiology to find a large blockage in one iliac while being entirely plaque free in the other. For this reason, no systems with a single large blockage were created for testing.

Part II: Methods and Results

Chapter 5: Methods

5.1 Experiments

The Omega transducers that were used in this project have four pins for wiring with the first three having connections and subsequent attached wires while the fourth pin with no connection is left alone. The first pin corresponds to the positive connection and is wired into the positive port in the 5 volt excitation source, while the second pin devoted to the negative connection is not only connected to the negative port in the excitation source but also a negative channel in the a/d board. The third pin representing the ground is connected to a positive channel on the a/d board. Once the wiring is complete the excitation source is turned on, allowing the transducers in conjunction with an acquisition program to record the necessary data.

The acquisition program used was a VI written in labVIEW. It was a simple program allowing the user to view the current pressure waveform and stop acquisition on command. The data would then be written to an excel sheet where it could be statistically analyzed against other data obtained. The curves were also placed into MATLAB to receive the Fast Fourier Transforms for each of the waveforms.

5.1.1 LabVIEW

The LabVIEW block diagram and front panel seen below in Figure 25 and Figure 26, respectively, was used to acquire data from the pressure transducers.

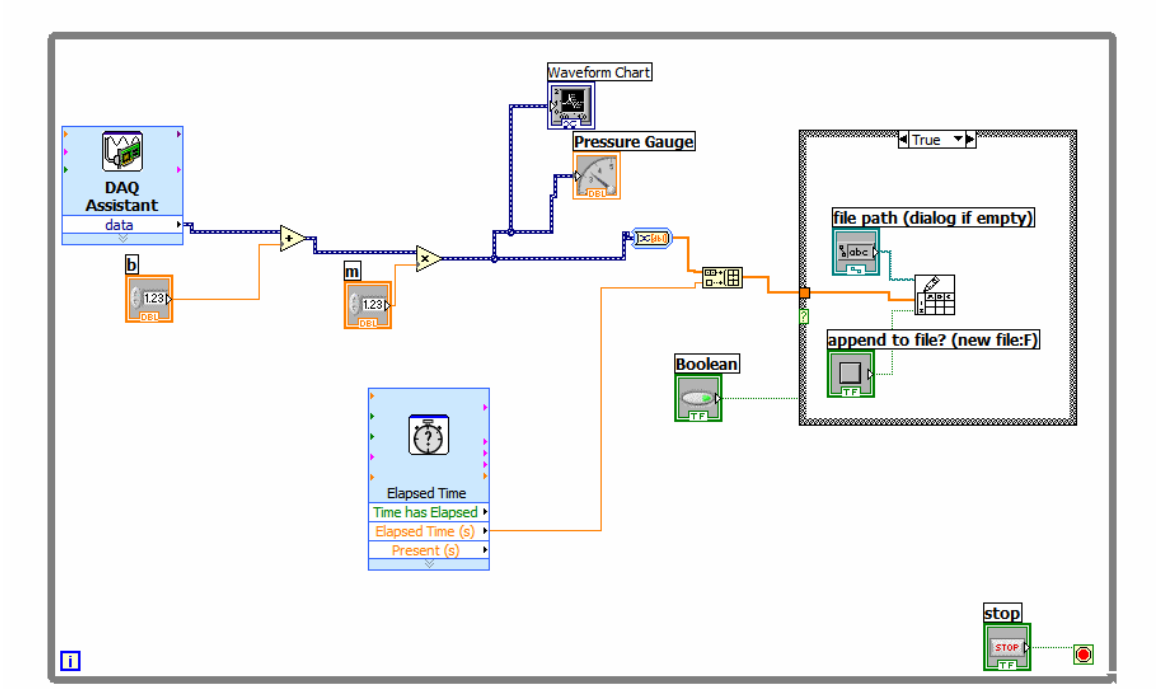

Figure 25: labVIEW block diagram

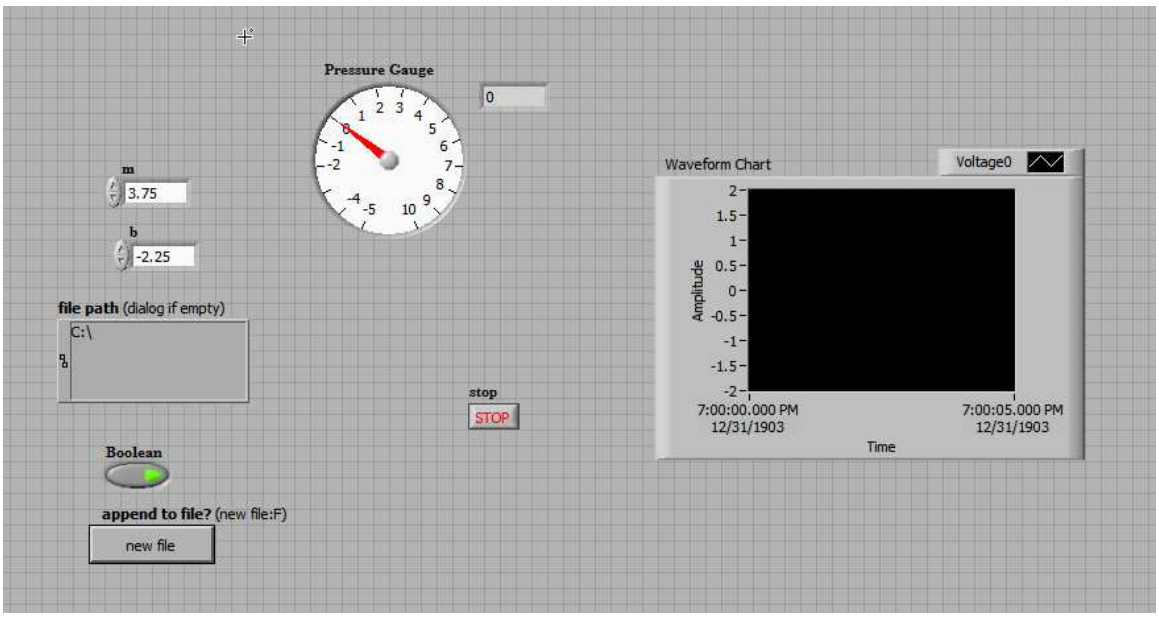

Figure 26: Labview front panel

Seen in Figure 25 is our calibration method for the transducers. The numeric value of -2.25 was added to the baseline data. This value would offset the baseline voltage of 2.25 that was being produced from the transducer. Next, 3.75 was inputted into the multiplier in order to convert the voltage readings into the pressure readings necessary to interpret our data. The file path allowed the directory to be chosen, and the

Boolean was used in order to have the LabVIEW program export the data into an excel file. This data was then analyzed in MATLAB.

5.1.2 MATLAB

MATLAB software was used to analyze the data that was exported into excel from LabVIEW. The data was imported into MATLAB from excel. From there, the code seen below was used to produce Fast Fourier Transform plots.

```
        Fs=input('Enter the Sampling frequency :')                  %
sampling frequency
        Fn=Fs/2;                  % Nyquist frequency
        %t=0:1/Fs:1;               % time vector sampled at Fs Hz,
                                  % length of 1 second
        %x = sin(2*pi*t*200);      % sine wave of 200 Hz.
        % Next highest power of 2 greater than or equal to
        % length(x):
         NFFT = 2^(nextpow2(length(x)))
        % Take fft, padding with zeros, length(FFTX)==NFFT
        FFTX=fft(x,NFFT);
        NumUniquePts = ceil((NFFT+1)/2);
        % fft is symmetric, throw away second half
        FFTX=FFTX(1:NumUniquePts);
        MX=abs(FFTX);            % Take magnitude of X
        % Multiply by 2 to take into account the fact that we
        % threw out second half of FFTX above
        MX=MX*2;
        MX(1)=MX(1)/2;   % Account for endpoint uniqueness
        MX(length(MX))=MX(length(MX))/2;  % We know NFFT is even
        % Scale the FFT so that it is not a function of the
        % length of x.
        MX=MX/length(x);                  %
        f=(0:NumUniquePts-1)*2*Fn/NFFT;
        plot(f,MX)
```

Chapter 6: Results

6.1 Pressure Waveform

The data obtained from the pressure transducers was plotted in excel to produce a pressure waveform. A plot was obtained from each trial of the varying blockages and can be found in the Appendices. The period of the waveform with the least noise was taken from each of these plots and graphed together as shown in Figure 27 below.

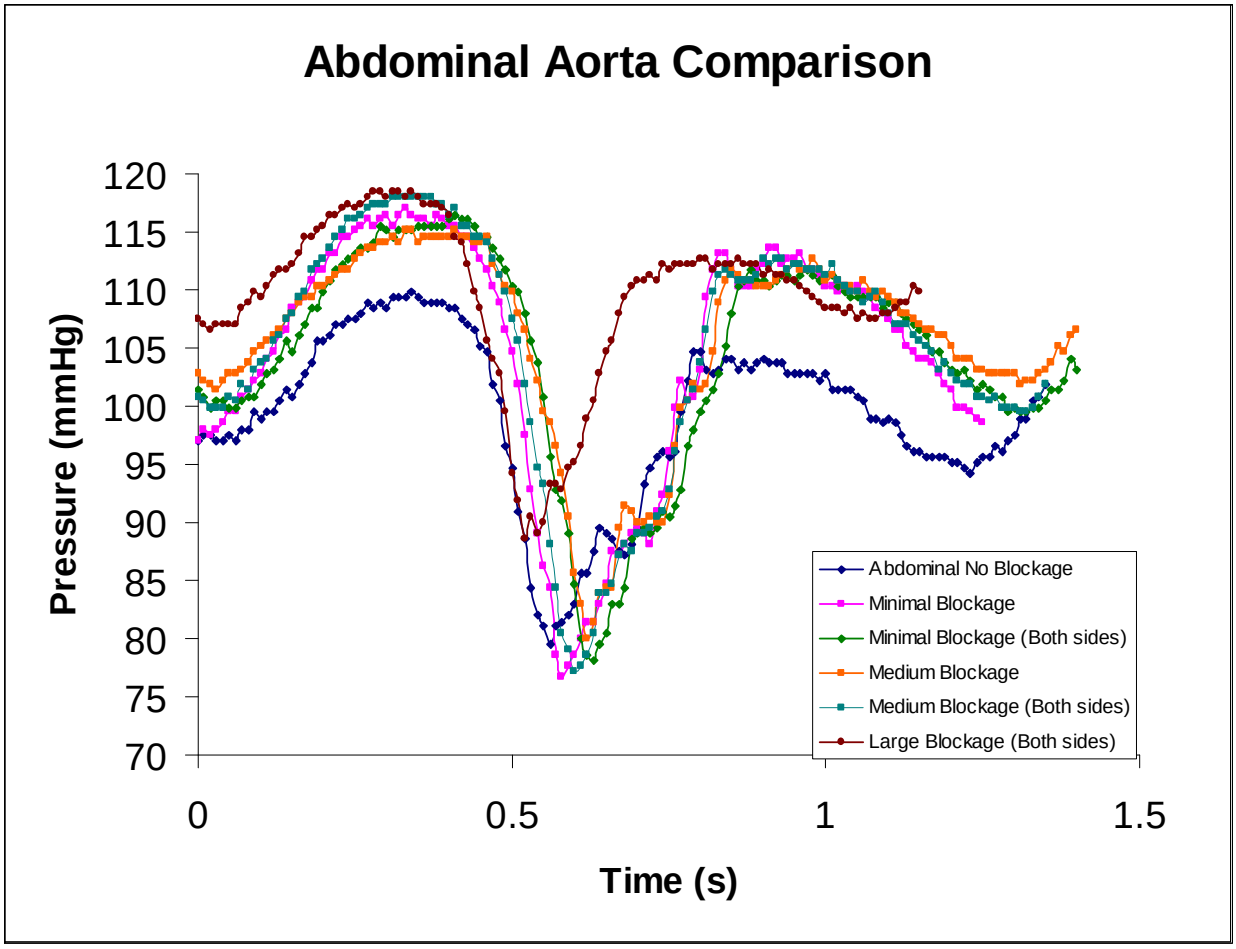

Figure 27: Plot of one period of pressure data from each of the varying degrees of blockages

The lack of analyzed iliac pressure data was due to the poor pressure waveforms gathered which contained too much noise, lacking the clarity needed to run the statistical analysis performed on the abdominal waveform, and FFT. Shown below in Figure 28 is an example of acquired iliac data.

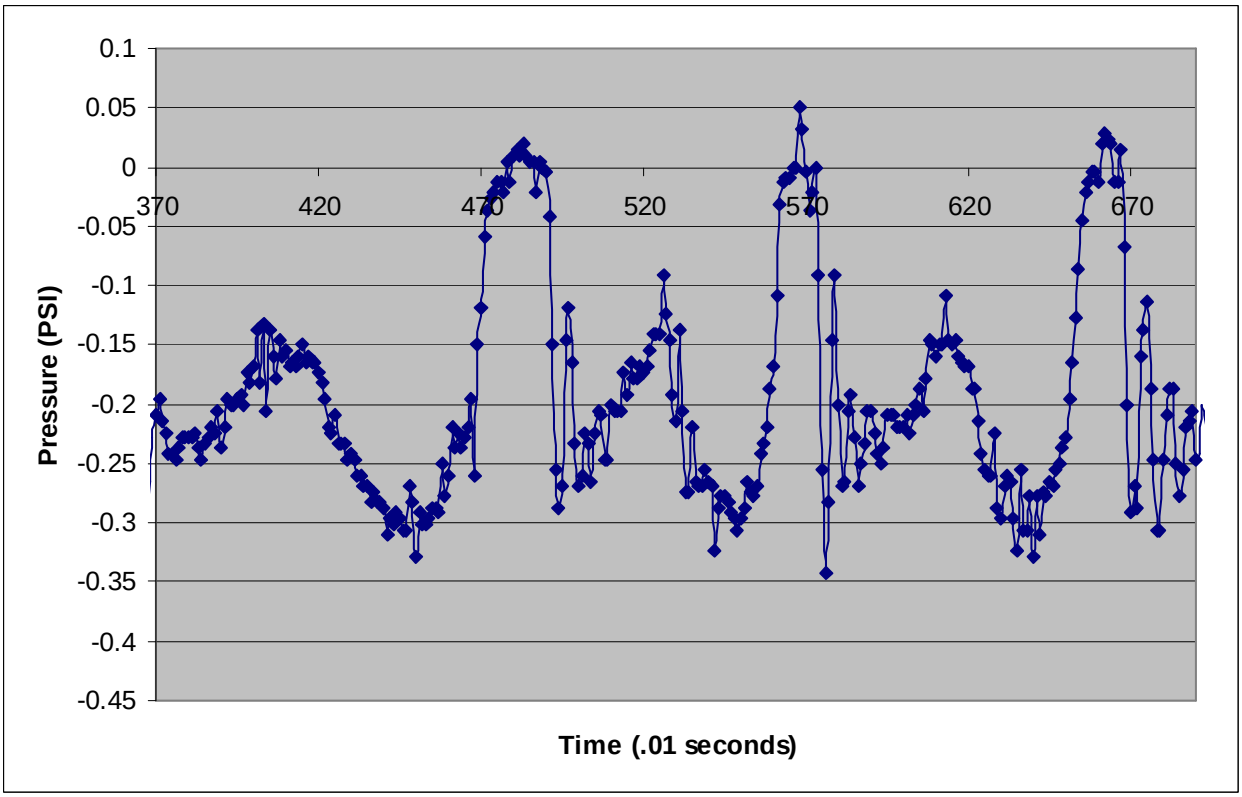

Figure 28: Three periods of a normal iliac waveform

6.2 FFT Results

The data obtained from the pressure transducers, after plotted as a waveform, was transferred from an Excel sheet into MatLab for FFT analysis. The data obtained from the trial of each artery system was analyzed using FFT and the graphs can be found in the Appendices. Shown below in Figure 28 is the FFT analysis of the data obtained from the abdominal artery in an unblocked artery system. The plot depicts five peak frequencies at frequencies of approximately 0, 1, 2, 3, and 4.

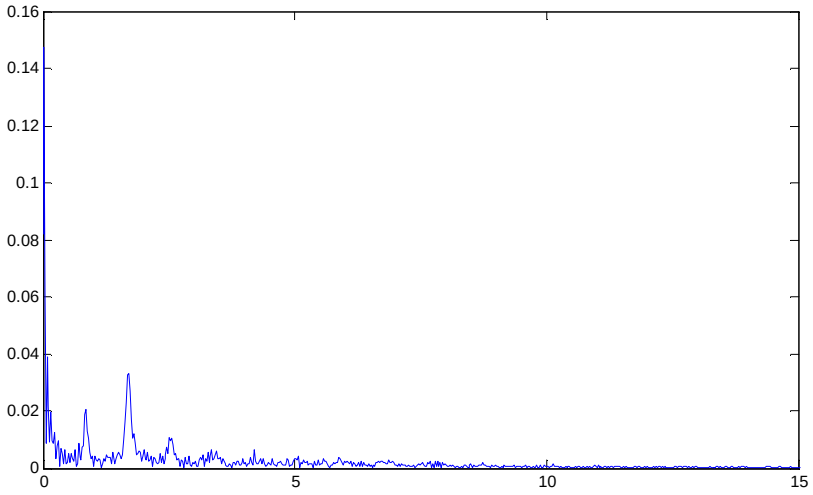

Figure 29:FFT amalysis of pressure in unblocked artery system

Similar to these results is the FFT of the abdominal aorta pressure waveform resulting from one minimally occluded iliac artery, as shown below in Figure 30. This graph also shows five peak frequencies.

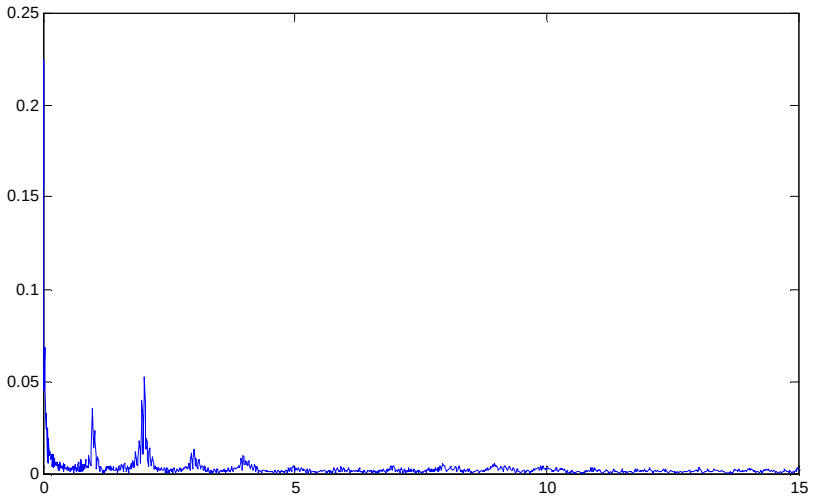

Figure 30: Pressure FFT of abdominal aorta with one minimally occluded iliac artery

Figure 31 shows the FFT of the abdominal aorta with both iliac arteries minimally occluded. Again, five peak frequencies can be observed, although not as clear as the previous two FFT plots.

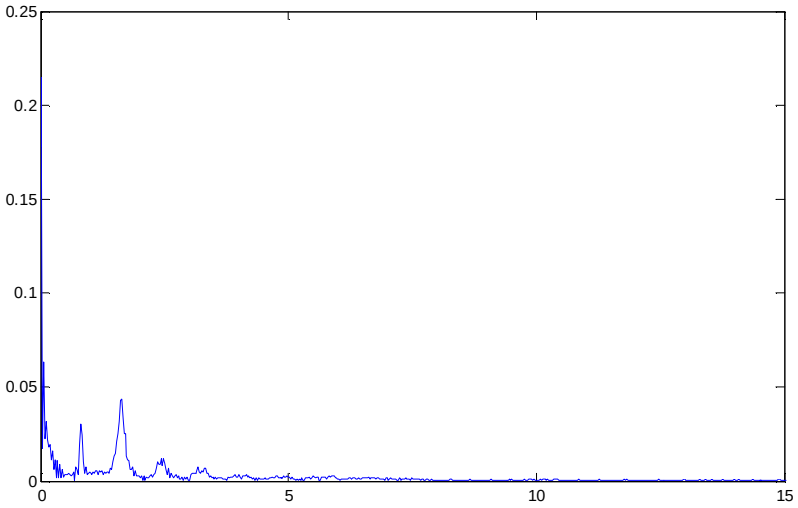

Figure 31: Pressure FFT of abdominal aorta with both iliac arteries minimally occluded

To provide a means of comparison, shown below in Figure 32 is the FFT of the abdominal aorta with a large blockage in each iliac artery.

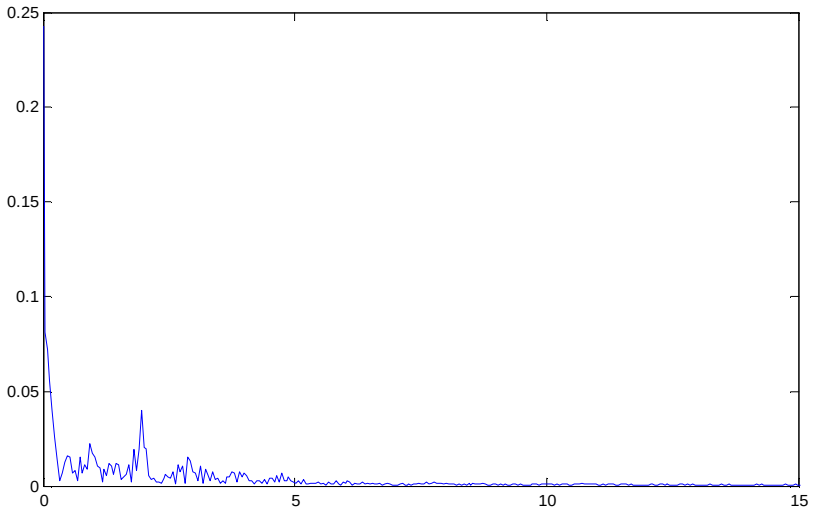

Figure 32: Pressure FFT of abdominal aorta with both iliac arteries mostly occluded

6.3 Statistical Results

Each pressure waveform obtained from output data of the pressure transducers was divided into four regions. The mean, and standard deviation were found for each degree of occlusion, and can be found in Table 10 below.

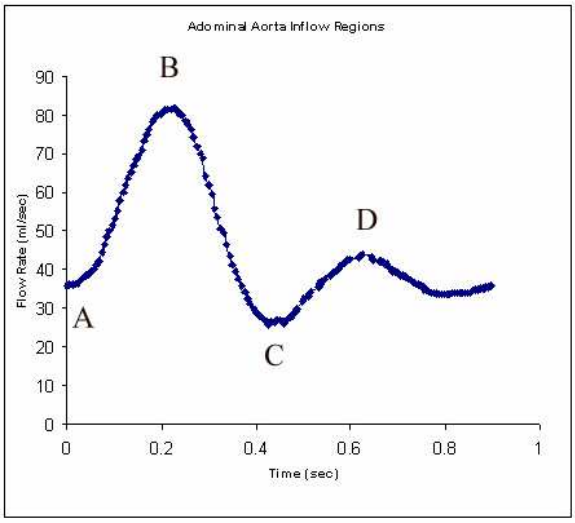

Figure 33: Labeled Regions of the Pressure Wave

Table 10: Averages and standard deviations of the varying degrees of iliac occlusion

	A	B	C	D
UNBLOCKED	0.012 ± 0.026	0.28 ± 0.026	0.19 ± 0.035	0.31 ± 0.025
MIN	-0.019 ± 0.016	0.32 ± 0.031	0.19 ± 0.019	0.35 ± 0.023
MED	0.0018 ± 0.012	0.31 ± 0.007	0.21 ± 0.006	0.34 ± 0.010
MIN-MIN	-0.020 ± 0.0048	0.31 ± 0.0060	0.19 ± 0.0077	0.35 ± 0.0029
MED-MED	0.023 ± 0.043	0.30 ± 0.024	0.20 ± 0.014	0.34 ± 0.023
LARGE	0.077 ± 0.016	0.32 ± 0.0044	0.2608 ± 0.0044	0.3698 ± 0.0039

Each degree of occlusion was compared against the control, the unblocked iliac arteries system, using an unpaired, one-tailed T-test. The results of these T-tests can be seen in Table 11 below. Each number that is below 0.05 is considered statistically significant.

Table 11: T test values for varying degrees of iliac occlusion

	A	B	C	D
MIN	6.77E-06	1.30E-06	2.62E-01	2.42E-07
MED	1.63E-02	3.64E-09	4.34E-05	3.64E-09
MIN-MIN	7.91E-05	2.93E-05	4.23E-01	6.33E-06
MED-MED	1.53E-01	7.83E-03	3.49E-02	1.13E-04
LARGE	1.65E-08	2.22E-05	8.18E-08	2.19E-08

The waveforms that were gained from the tranducer readings had FFT performed on them and the means and the standard deviations of each of the harmonics were taken and are shown below in Table 12.

Table 12: The mean and standard deviation of each harmonic

	ω0	ω1	ω2	ω3	ω4	ω5
clear	0.21 ± 0.055	0.030 ± 0.012	0.036 ± 0.0035	0.011 ± 0.0016	0.0058 ± 0.0016	0.0041 ± 0.0020
minimal blockage	0.21 ± 0.016	0.034 ± 0.002	0.062 ± 0.0084	0.018 ± 0.0047	0.010 ± 0.0025	0.0053 ± 0.00085
medium blockage	0.23 ± 0.0073	0.028 ± 0.0058	0.044 ± 0.0099	0.014 ± 0.0040	0.0079 ± 0.0014	0.0035 ± 0.00087
2 minimal blockages	0.23 ± 0.020	0.052 ± 0.018	0.11 ± 0.0080	0.033 ± 0.0055	0.023 ± 0.013	0.013 ± 0.0078
2 medium blockages	0.23 ± 0.0059	0.044 ± 0.0043	0.077 ± 0.012	0.027 ± 0.0027	0.016 ± 0.011	0.010 ±0.0027
huge blockage	0.28 ± 0.0019	0.058 ±0.0074	0.076 ± 0.0066	0.029 ± 0.0062	0.020 ± 0.0037	0.0105 ± 0.0038

The harmonic amplitudes of each degree of occlusion were compared against the control harmonic amplitudes of the unblocked iliac arteries system, using an unpaired, one-tailed T-test similar to the fashion in which the regions were compared. The results of these T-tests can be seen in Table 13 below. Each number that is below 0.05 is considered statistically significant.

Table 13: The T test values for each of the harmonics

	ω0	ω1	ω2	ω3	ω4	ω5
minimal blockage	0.4872	0.3309	0.0043	0.0428	0.0304	0.2004
medium blockage	0.3151	0.3999	0.1469	0.2022	0.0802	0.3295
2 minimal blockages	0.3239	0.0766	0.0001	0.0014	0.0444	0.0589
2 medium blockages	0.2603	0.0652	0.0025	0.0005	0.0857	0.0165
large blockage	0.0431	0.0129	0.0004	0.0040	0.0017	0.0301

Chapter 7: Analysis and Discussion

7.1 Pressure Waveform

The plot of the pressure waveforms found in Figure 27 demonstrates a generally upwards trend in pressure. The pressure of the arterials system with no blockages can typically been seen to be less than the waveforms of the occluded systems. The two maximum pressures of the occluded iliac artery systems seem to be significantly higher than that of the control. Although the local minimums of the occluded vessels show an overall increase in pressure, the minimum does not. The minimum pressures of these waveforms seem to be inconsistent at best. A majority of the occluded vessel's minimum pressures are less than that of the control, with the exception of the largely occluded iliac

arteries. With the exception of the minimum value, the pressure waveforms demonstrate a positive shift in pressure as the occlusions get larger.

7.2 FFT

When determining the equation of the curve used to calculate the shape of the cam, the digitized points yielded an equation with 10 harmonics. Although similar studies have been done with anywhere from five to ten harmonics, ten harmonics was used in this instance, to ensure better results.

The plot in Figure 29 depicts five peak frequencies at frequencies of approximately 0, 1, 2, 3, and 4. The amplitude peaks do not fall exactly on frequencies 0, 1, 2, 3 and 4, most likely because the rotation of the cam may have been slightly off. Combine two sentences. The cam was to rotate at approximately 60 rpms, but this may have been slightly off, causing the amplitude peaks of the FFT to be shifted. This indicates that 5 harmonics would correctly mimic the flow curve of this data. The FFT shown in Figure 30, similar to that of Figure 29, again depicts 5 peak amplitudes at the same frequencies, corresponding to 5 harmonics. The amplitude values of the FFT of the minimally occluded artery are slightly smaller than that of the unblocked artery. Figure 31, likewise, demonstrates five harmonics, although not quite as clear as the first two FFT plots.

The FFT of the largely occluded iliac arteries is quite different than that of the first three FFTs. The FFT shown in Figure 32 has no discernable amplitudes, making it difficult to determine the harmonics of the flow. There are no clear harmonics for this plot. The FFT has much more noise and variance than the first three. One possible explanation for this difference may be a result of turbulent flow due to the large blockages in the iliac arteries.

7.3 Statistical Significance

As Table 10 demonstrates, a majority of the T test results are less than 0.05, deeming them statistically significant. As expected, all of the largely occluded systems were found to be statistically significant. Three of the calculated T tests were not statistically significant: a minimal occlusion, minimal occlusions in both iliac arteries and

medium occlusions in both iliac arteries. Since only one region of the waveform for 3 different occlusion degrees was found to not be statistically significant, it can be assumed that the overall waveform is statistically significant. The lack of significance in these three tests may be a result of human error, or an experiment containing large outliers, affecting the statistic calculations.

Unlike the results for the region testing the statistical significance of the Fast Fourier Transforms are less consistent. The first and second harmonic amplitudes were not significant in any of the blockages except for the symptomatic large blockage. The third and fourth harmonic amplitudes however, were only not significant in the medium blockage, while the fifth harmonic amplitude was significant in the minimum blockages in both, the medium blockages in both, and the large symptomatic blockages. The reason for the lack of significance, and high standard deviations in the medium for the third and fourth harmonic amplitudes was possibly due variability in our test methods.

Chapter 8: Conclusions

There are several distinct conclusions that can be drawn from this project. This section will address these conclusions as suggested by the data and also examine their implications to the bigger issue.

The first conclusion suggested by the time waveform of pressure data was that the only statistically significant changes in pressure can be found in arteries that contain large blockages. This also implies that techniques used to detect these types of blockages would not be clinically useful. Developing that technology would not be a good investment because at this stage of atherosclerosis, the changes in pressure would already be manifesting in physical symptoms. By the time the changes in pressure could be detected non-invasively, the disease would already present in symptoms such as chest pain, stroke, embolism, or possibly even death.

The next conclusion suggested by the data was that statistical analysis of the pressure curves showed that minimal and medium blockages can be detected based on changes in flow. Although three of the T-tests produced results that were not statistically significant, the pressure waveform can still be considered to be statistically significant. This conclusion implies that a non-invasive technique may be able to detect minimal or medium sized blockages based on pressure readings.

Chapter 9: Recommendations

Throughout the course of this project, many ideas presented themselves which could have taken the project in a different direction. Those ideas will be given in this section as recommendations to enhance or redirect this project in the future. First, various pathologies will be discussed, followed by possible ranges of biological circumstances.

While this project primarily examined the various stages of atherosclerosis, there are many other conditions which affect flow in the arteries. When atherosclerosis reaches a critical state, medical devices called stents are sometimes introduced into the artery to regain unobstructed blood flow. These stents are shaped in a mesh tube and used to mechanically prop open the occluded vessel. Occasionally smooth muscle cells can re-grow over the sides of the stent, resulting in restenosis of the artery. Both of these cases could be investigated in future studies, examining the flow of stented and restenosed arteries versus healthy ones.

Another pathology sometimes found in the abdominal aorta and iliac arteries is the aneurysm. This occurs when a weakening in the artery wall cannot maintain its structural integrity in the high pressure flow. The artery balloons out, allowing for the pooling of excess blood which certainly adds turbulence to the downstream iliac flow. By varying the elastic modulus, and compliance, of the abdominal aorta, the project could be changed to study the effects of aneurysms on flow.

A third condition, a vascular graft, is often a result of an aneurysm. When an aneurysm or mechanical instability is detected in the abdominal aorta, doctors can elect to replace the vessel with a graft. Materials currently used in grafts try to match the compliance of natural arteries, but do not always succeed. This project could also be used to study the effects of compliance changes between natural and grafted vessels and their subsequent effects on flow.

In addition to examining various biological pathologies, this project could be used to investigate the changes in flow resulting from different physical conditions. Stroke volume and heart rate are two conditions that could be looked at, as normal physical activities could affect either. The stroke volume of the system could be varied by manufacturing different sized cams. This would increase or decrease the length the piston head traveled and ultimately the volume of fluid displaced in the system.

Heart rate can greatly affect the amount of pressure and strain placed on the arteries. In the system, varying the speed of the motor, and thus the cam, could simulate physiological conditions during exercise or rest. In this project, the rate examined was 60bmp or 1Hz. During exercise, the human body can experience average heart rates reaching into the 120-140 bmp. The project could look at the changes in frequency under 2Hz and compare them to the values obtained at 1Hz. It could be interesting to see if the statistical significance of the data was changed with increases in heart rate.

References

1. American Heart Association. *Cardiovascular Disease Statistics*. 2006. 16 Nov. 2006 Available online at: http://www.americanheart.org/presenter.jhtml?identifier=4478.
2. Davies, John R., Rudd, James H., Weissberg, Peter L. Molecular and Metabolic Imaging of Atherolsclerosis. *The Journal of Nuclear Medicine.* 45:11 1898-1907. 2004.
3. R. Lloyd. Synthetic Blood Vessels Not Such a Stretch. LiveScience Health SciTech. Available 21 Novemeber 2006 online at: http://www.livescience.com/humanbiology/060619_synthetic_arteries.html
4. Thierry, B., et al. *Stents*. Encyclopedia of Biomaterials and Biomedical Engineering. 2004.
5. Burt, H., et al. *Drug-eluting stents: A multidisciplinary success story*. Advanced Drug Delivery Reviews. Vol. 58, 350-357, 2006.
6. Angioplasty. *Medline Plus: National Institutes of Health*. Available online at: http://www.nlm.nih.gov/medlineplus/ency/article/002953.htm. 2006. Accessed Nov 29, 2006.
7. Heart Health Online. *Stents*. FDA. 27 Feb. 2004. Available online at: http://www.accessdata.fda.gov/scripts/cdrh/cfdocs/cfTopic/mda/mda-. Accessed Nov 12, 2006.
8. Stent. Guidant. Available online at: http://www.guidant.com/condition/pop30.html. Accessed Nov 29, 2006.
9. Restenosis. *OrbusNeich*. Available online at: http://www.orbusneich.com/patients/genous/glossary/page2.php?PHPSESSID=d3bf5eb0eed5f6a353d73c. Accessed Dec 1, 2006.
10. S. Kolluri. (1991) A noninvasive technique for early detection of atherosclerosis using the impedance plethysmograph: Longitudinal study on cynomolgus monkeys. UMI. Available online at: http://wwwlib.umi.com/dissertations/preview_page/9210160/1. 6 December 2006.
11. M Ogawa, S. Ishino, T. Mukai, D. Asano, N Teramoto, H. Watabe, N. Kudomi, M. Shiomi, Y. Magata, H. Iida, & H. Saji. (2004) ^{18}F-FDG Accumulation in Atherosclerotic Plaques: Immunohistochemical and PET Imaging Study. *Journal of Nuclear Medicine*. 45(7): 1245-1250.
12. M. Honda, I. Kawahara, N. Kitagawa, K. Tsutsumi, M. Morikawa, T. Hayashi, & I. Nagata. (2006) Asymptomatic carotid artery plaques: use of magnetic resonance imaging to characterize vulnerable plaques in 6 cases. *Surgical Neurology*. Article in Press.
13. S.G. Ruehm, M. Goyen, J. Barkhausen, K. Kroger, S. Bosk, M.E. Ladd, & J.F. Debatin. (2001) Rapid magnetic resonance angiography for detection of athersclerosis. *Lancet* 357:1086-91.
14. T. Miyazaki, K. Shimada, O. Sato, K. Kotani, A. Kume, K. Sumiyoshi, Y. Sato, H. Ohmura, Y. Watanabe, H. Mokuno, & H. Daida. (2005) Circulating

malondialdehyde-modified LDL atherogenic lipoprotein profiles measured by nuclear magnetic resonance spectroscopy in patients with coronary artery disease. *Atherosclerosis*. 179(1):139-145.
15. O.Y. Atkov, T.V. Balahonova, & O.A. Pogorelova. (1998) Non-invasive ultrasound detection of endothelial dysfunction. *European Journal of Ultrasound*. 7(1):37-45.
16. Definition of Abdominal Aorta. *MedicineNet.com.* Available online at: http://www.medterms.com/script/main/art.asp?articlekey=8631. Accessed Dec 2, 2006.
17. AAA Abdominal Aortic Aneurysm. *North County Radiology*. Available online at: http://www.northcountyrad.com/AAA-abdominal-aortic-aneurysm-tri-city-oceanside.htm. Accessed Nov 28, 2006.
18. Influence of anatomic distribution of atherosclerosis on the outcome of revascularization with iliac stent placement. *Journal of Vascular and Interventional Radiology*, Vol 6, Issue 4 513-521. 1995.
19. The Heart. *ScienceBob.com*. Available online at: http://www.sciencebob.com/lab/bodyzone/heart.html. Accessed Nov 28, 2006.
20. Davis, Nicole. Dept of Genetics, Harvard Medical School. Available online at: http://www.madsci.org/posts/archives/mar99/921961618.Me.r.html. Accessed Nov 29, 2006.
21. Maryann Anglim, Walter Allan, M.D.. *Kara Mia*. Bath, ME. 1977.
22. Taylor, Charles A., Hughes, Thomas J. R., Zarins, Christopher K. Finite Element Modeling of Three-Dimensional Pulsatile Flow in the Abdominal Aorta: Relevance to Atherosclerosis. *Annals of Biomedical Engineering*. 26 975-987, 1998.
23. Cam. *Wikipedia*. http://en.wikipedia.org/wiki/Cam. Accessed on Dec 2, 2006.
24. T.G. Beckwith, R.D. Marangoni, J.H Lienhard V. Mechanical Measurements. Pearson Education, Inc. Upper Saddle River, NJ. 2007. 6th ed.
25. J. Essick. Advanced LabVIEW Labs. Prentice-Hall, Inc. Upper Saddle River, NJ. 1999.
26. MATLAB Function Reference. The Mathworks. (2007). Available 12 December 2007 online at: http://www.mathworks.com/access/helpdesk/help/techdoc/index.html?/access/helpdesk/help/techdoc/ref/fft.html&http://www.google.com/search?hl=en&q=fft+matlab
27. FFT Analysis. National Instruments. (2007). Available 12 December 2007 online at: http://zone.ni.com/devzone/cda/tut/p/id/3342.

Appendices

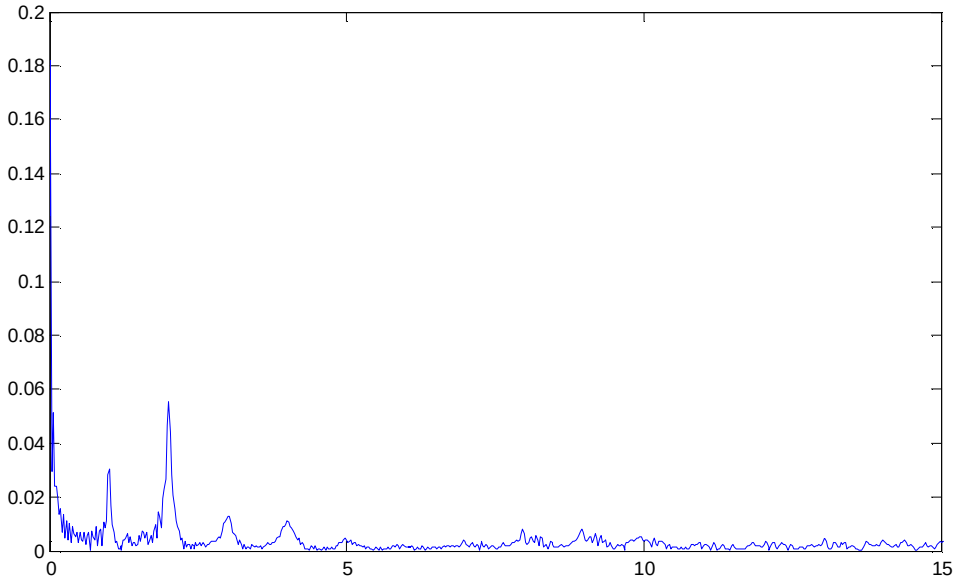

Figure 34:mqpsugarilliacLB1

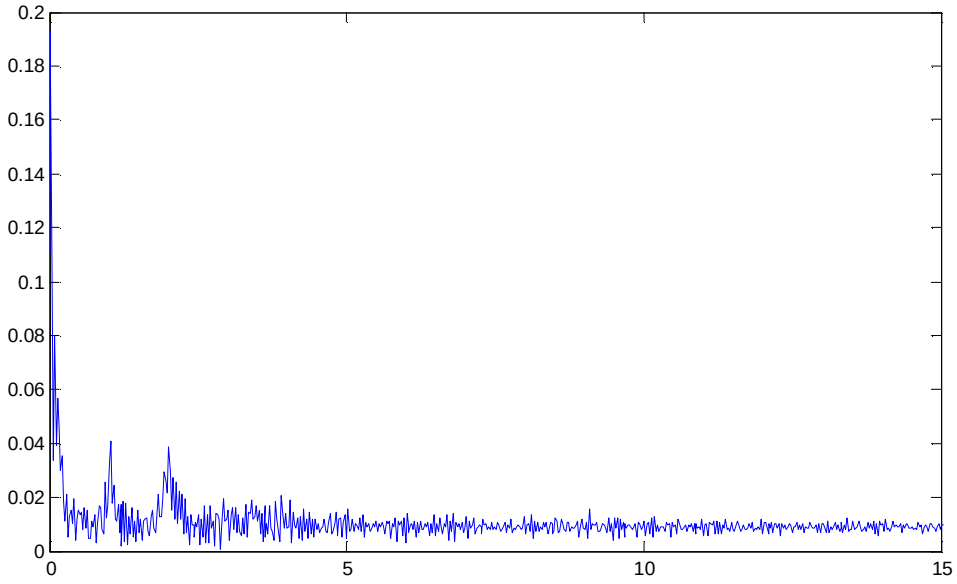

Figure 35:mqpsugarilliacLB2

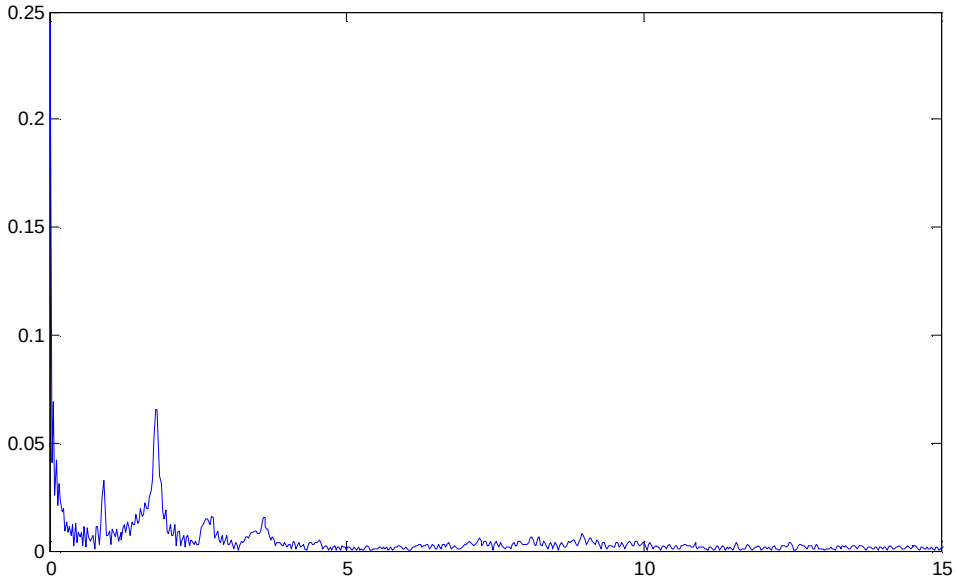

Figure 36:mqpsugarilliacLB3

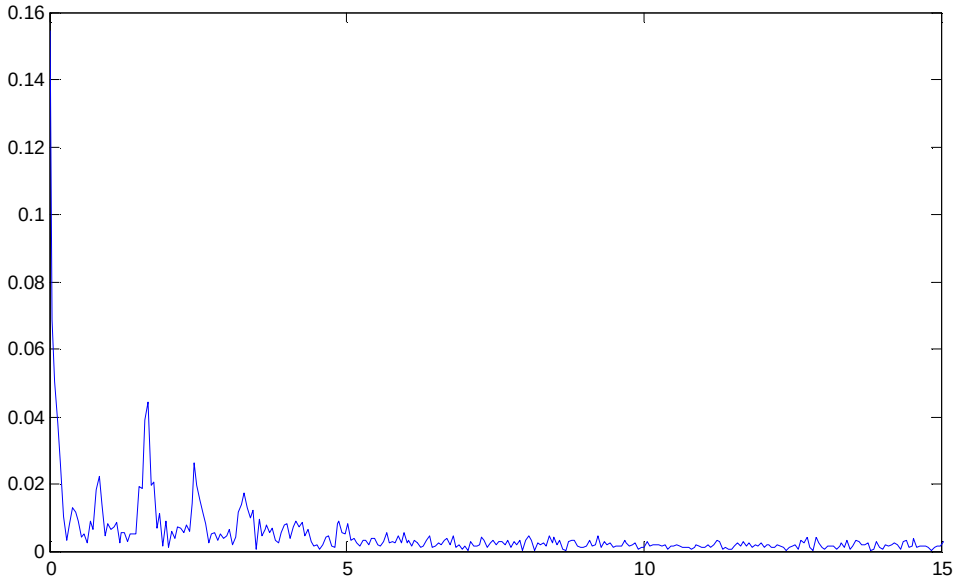

Figure 37:mqpsugarilliacMB3

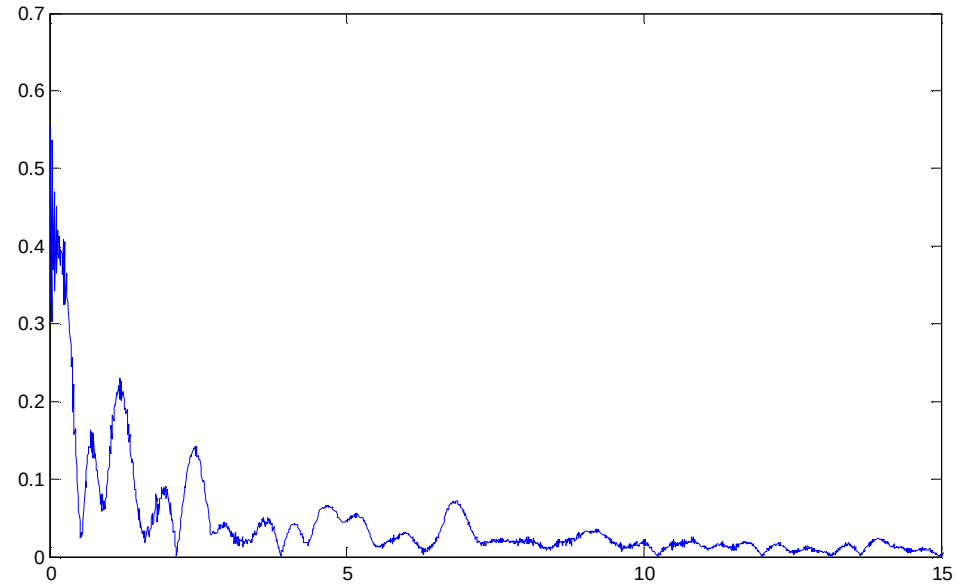

Figure 38:mqpsugarilliacMB2

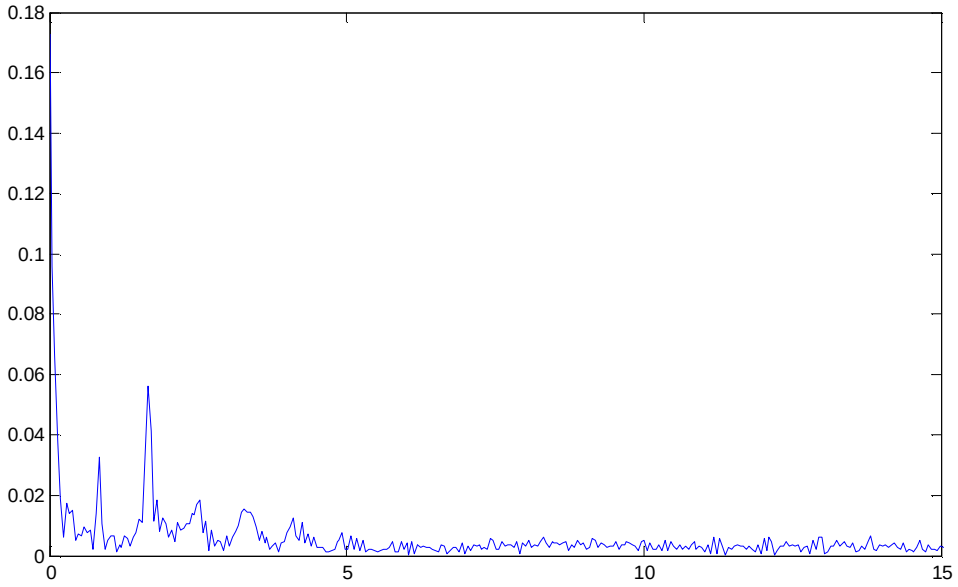

Figure 39:mqpsugarilliacMB1

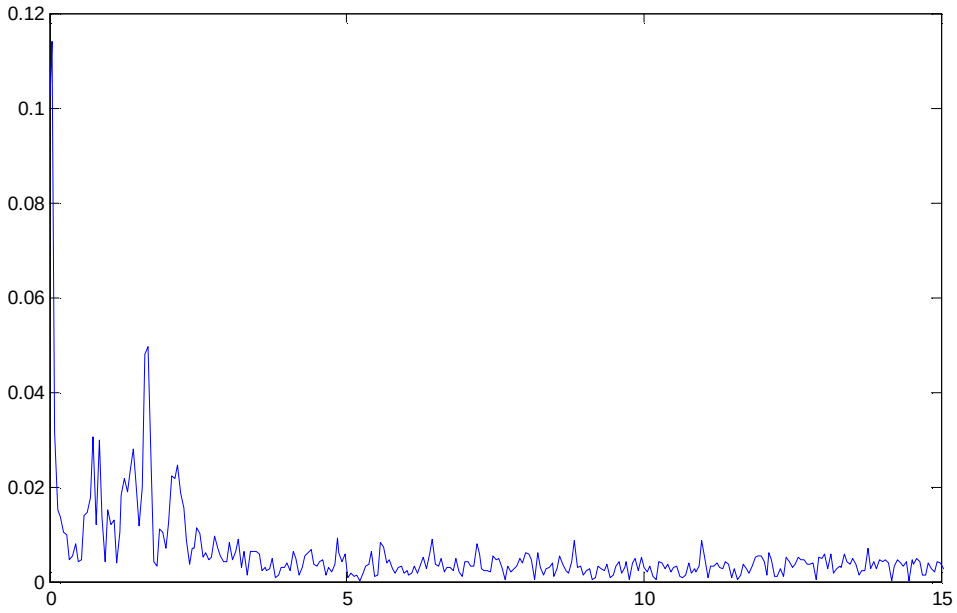

Figure 40:mqpsuagarilliac1

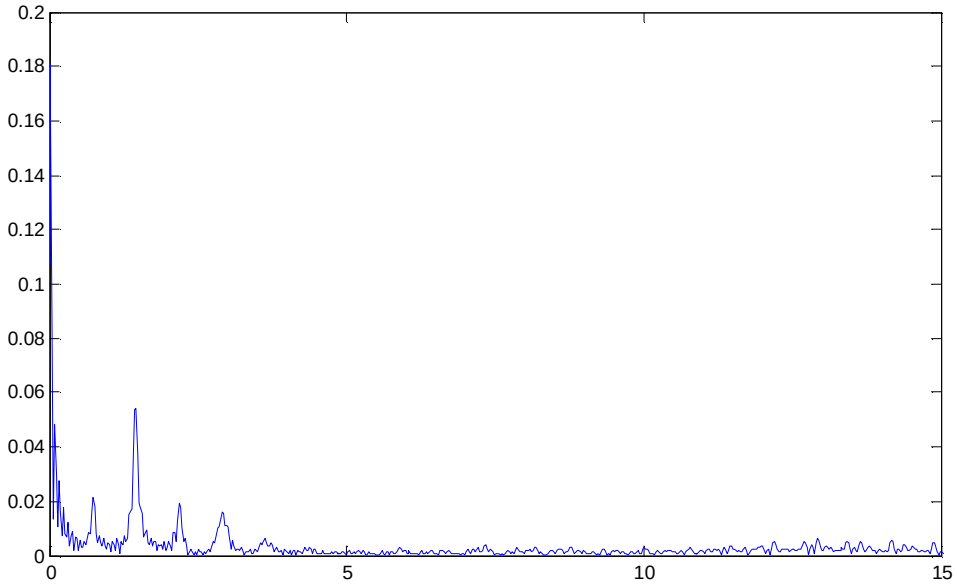

Figure 41:mqpsugarilliac2

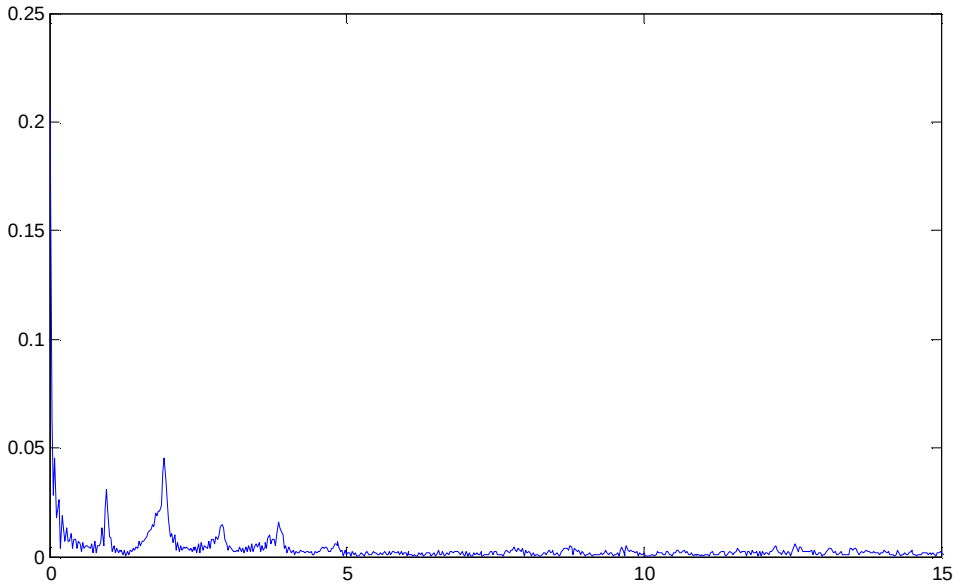

Figure 42:mqpsugarilliac3

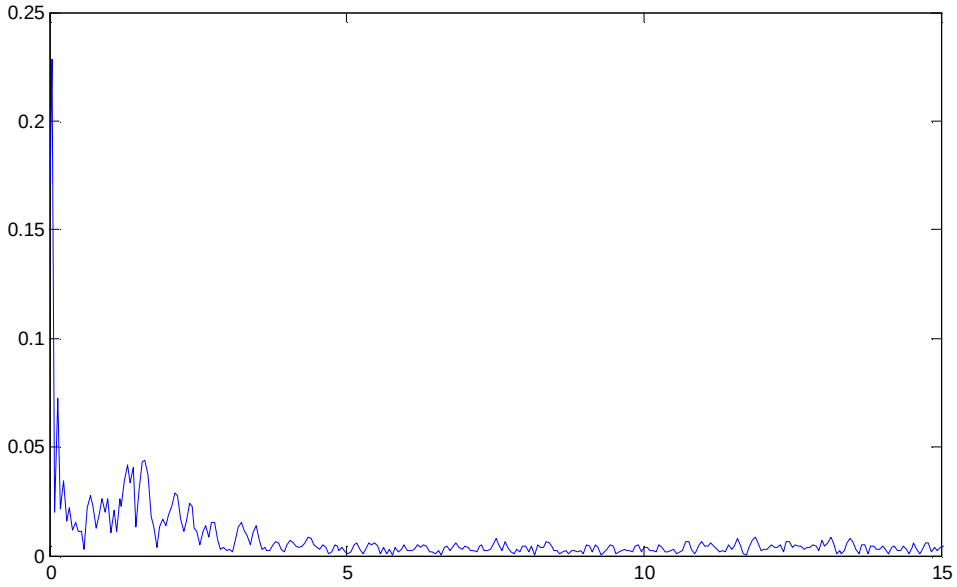

Figure 43:mqpsugarilliac1.5

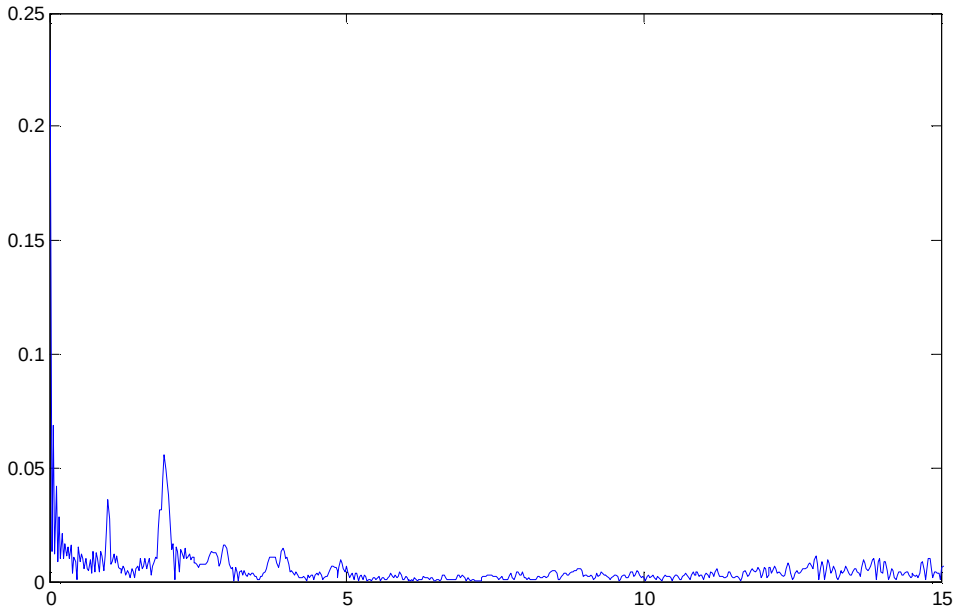

Figure 44:mqpsugarilliac2.5

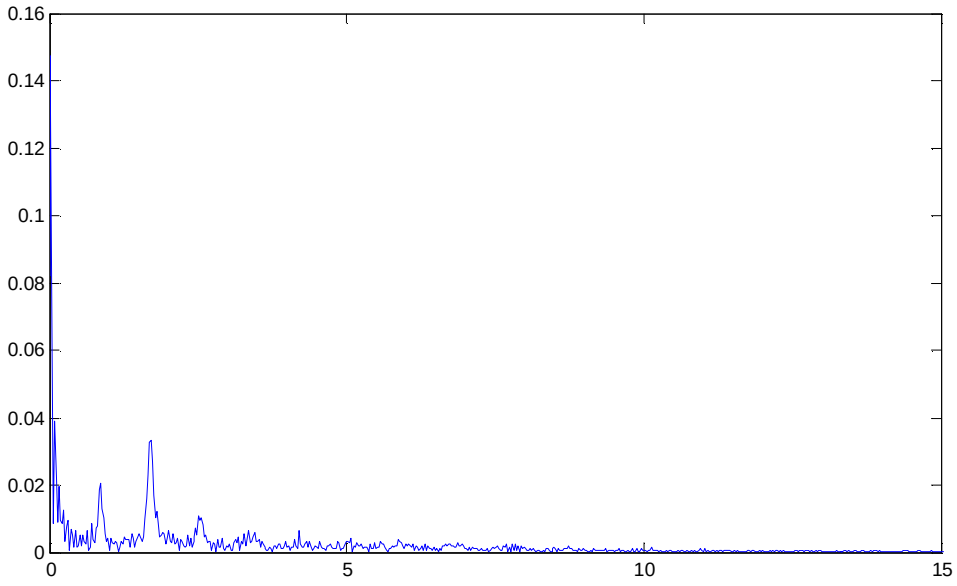

Figure 45:mqpsugarabdominal1

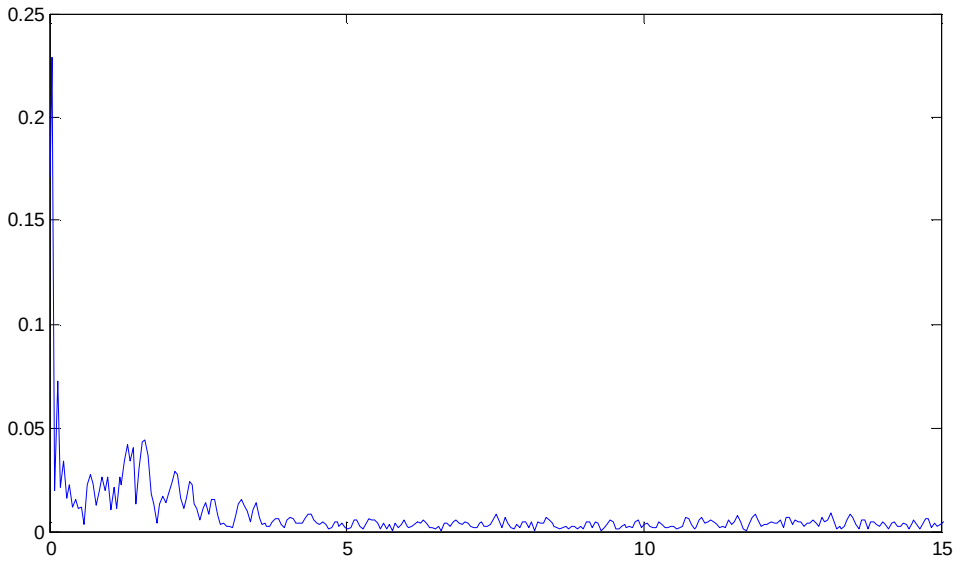

Figure 46:mqpsugarabdominal2

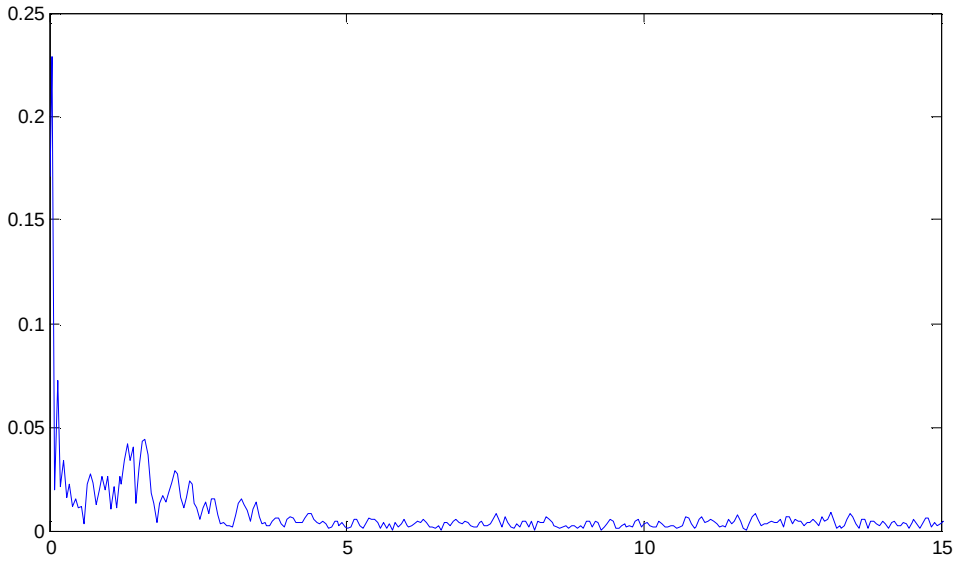

Figure 47:mqpsugarabdominal3

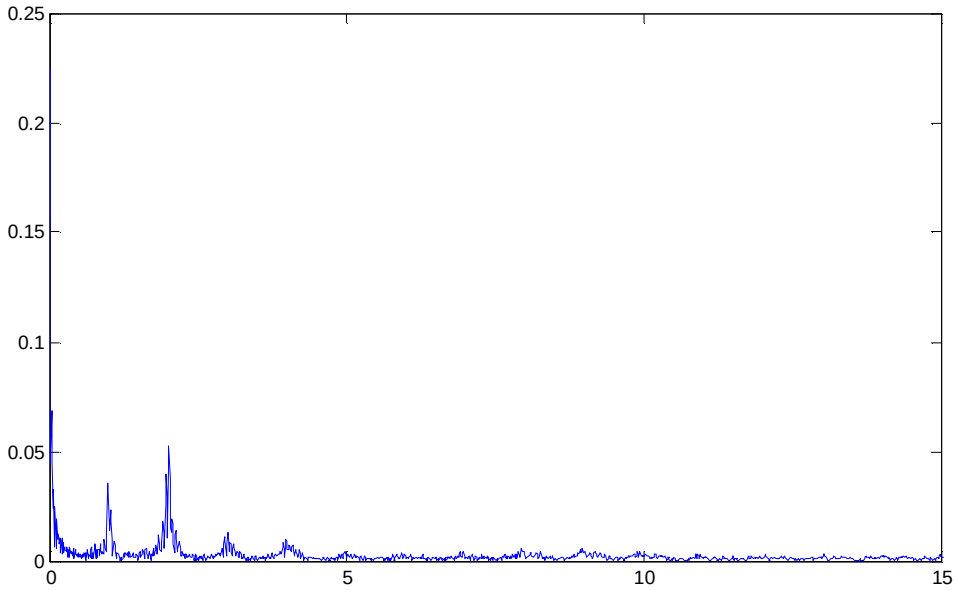

Figure 48:mqpsugarabdominal LB2

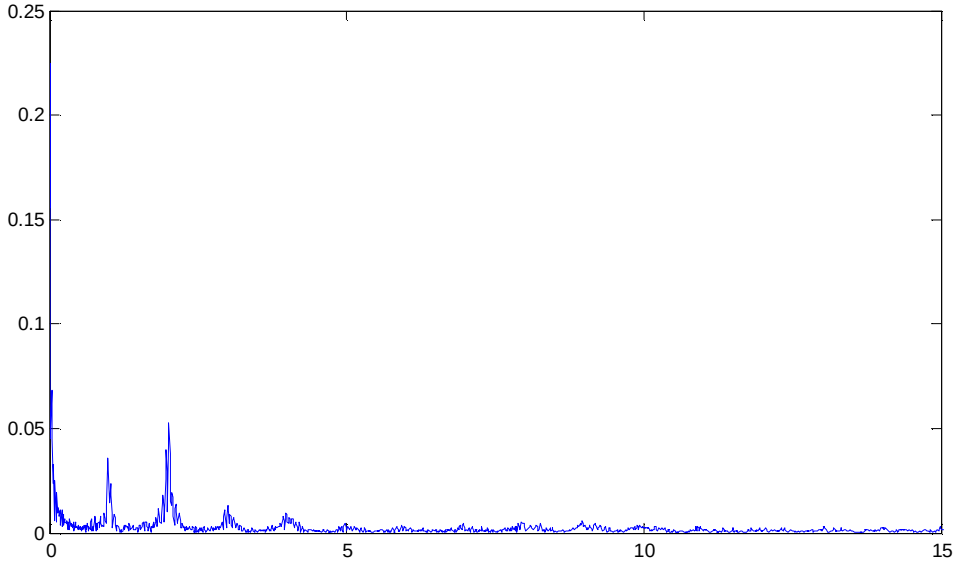

Figure 49:mqpsugarabdominalLB3

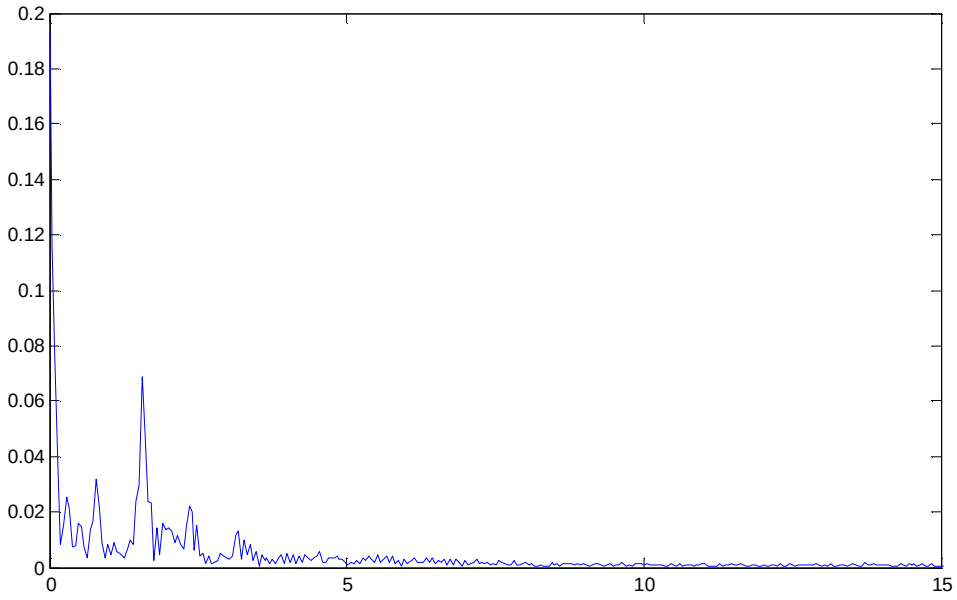

Figure 50:mqpsugarabdominalLB1

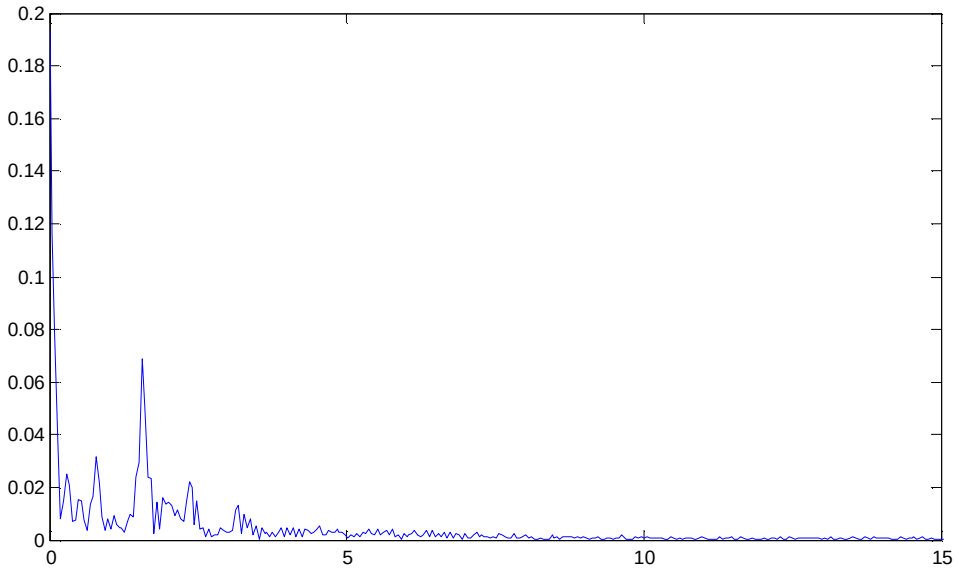

Figure 51:mqpsugarabdominalMB1

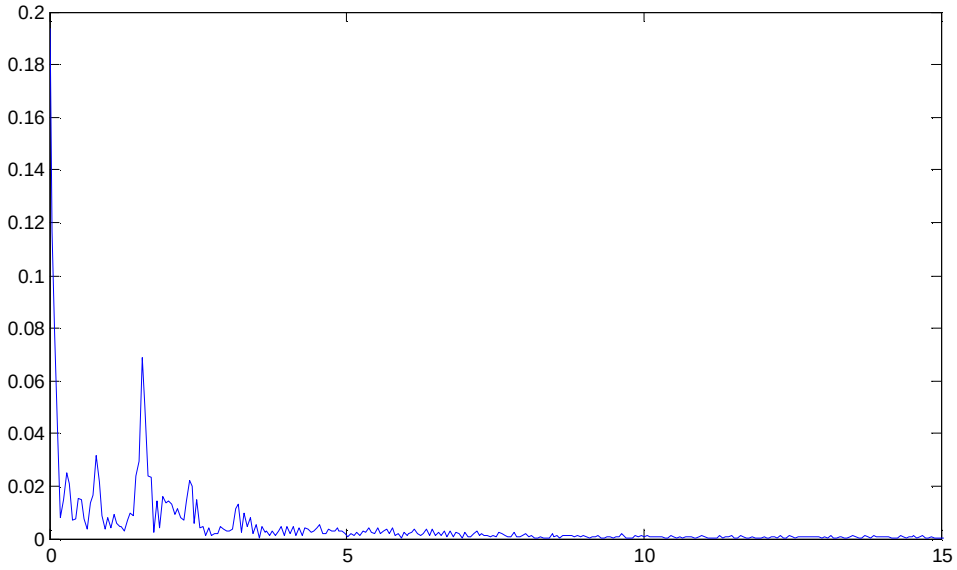

Figure 52:mqpsugarabdomnialMB2

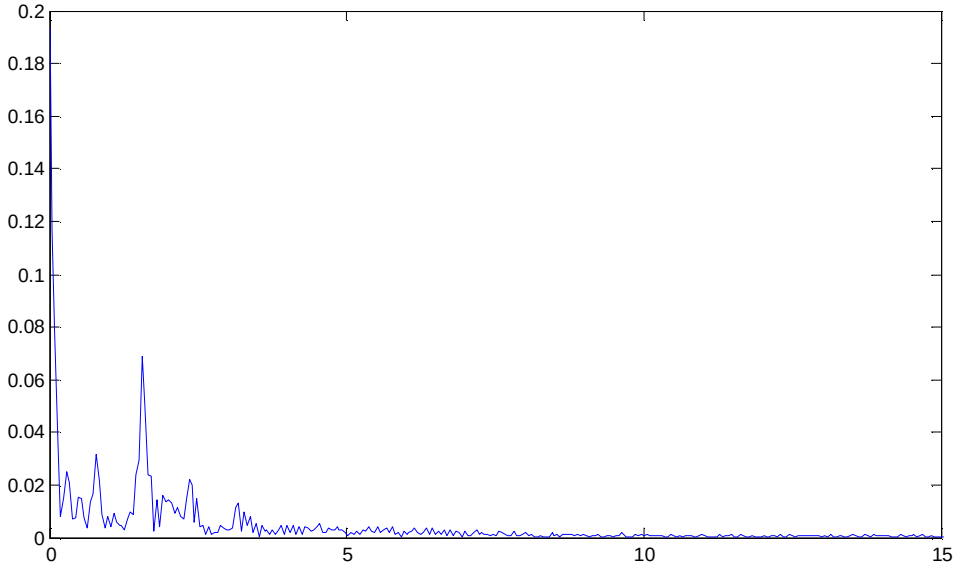

Figure 53:mqpsugarabdominalMB3

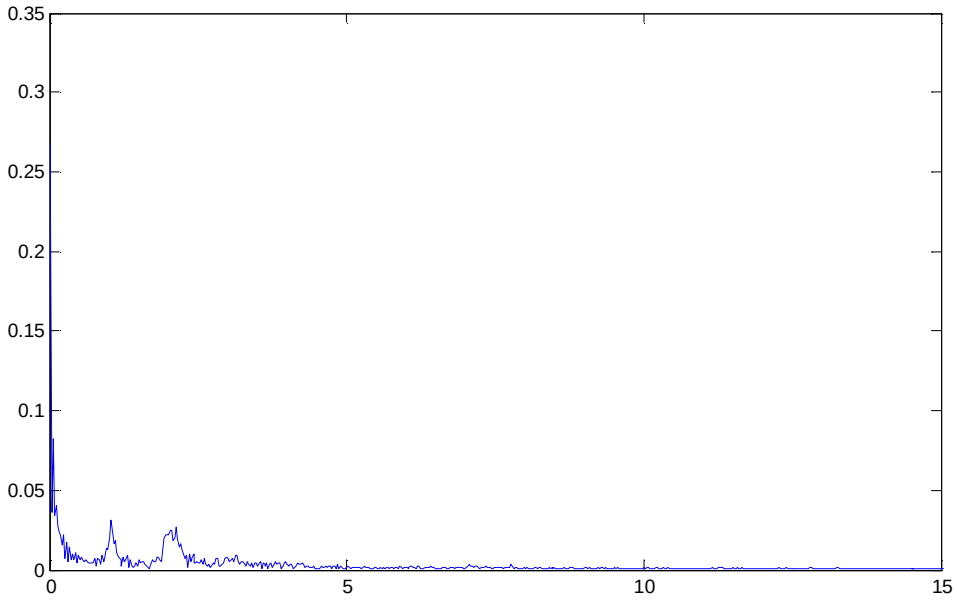

Figure 54:Med+Med abdominal1

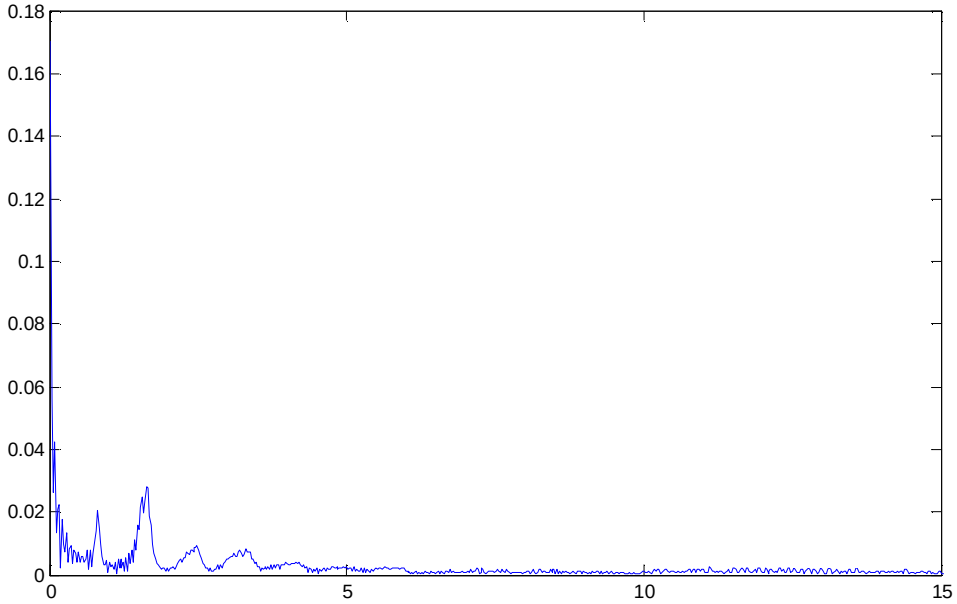

Figure 55:Med+Med illiac 1

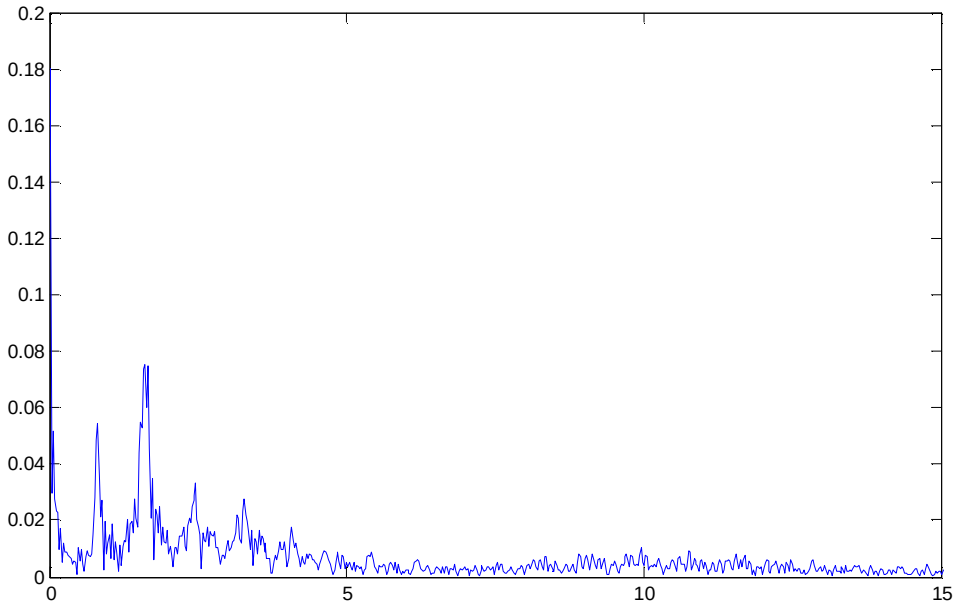

Figure 56:Med+Med illiac 2

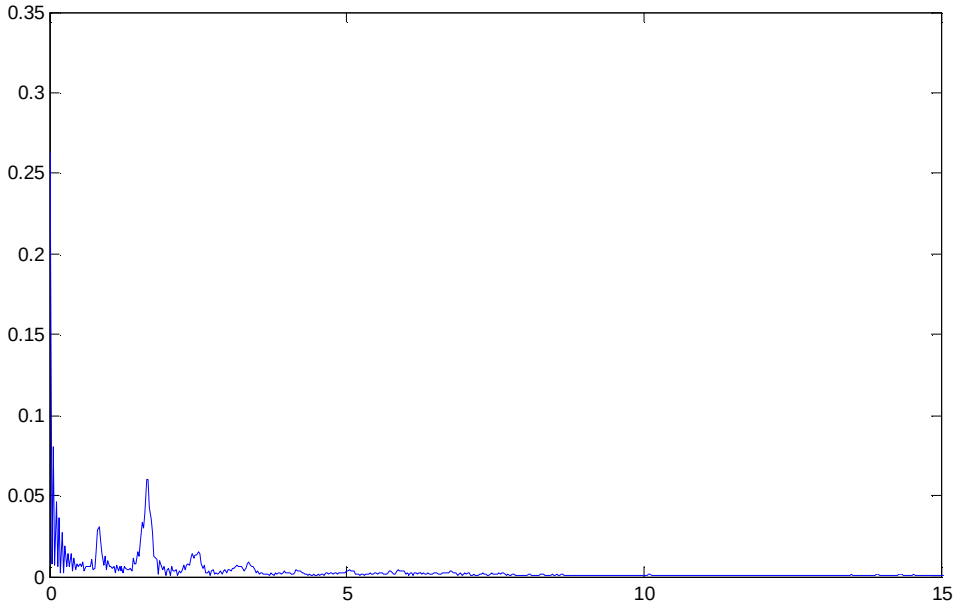

Figure 57:Med+Med abdominal 2

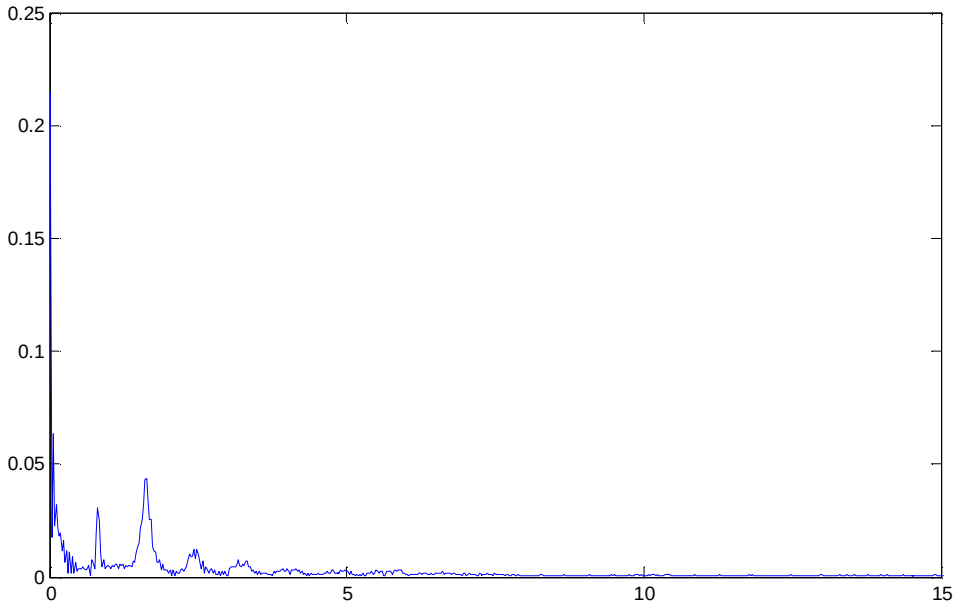

Figure 58:Min+Min abdominal

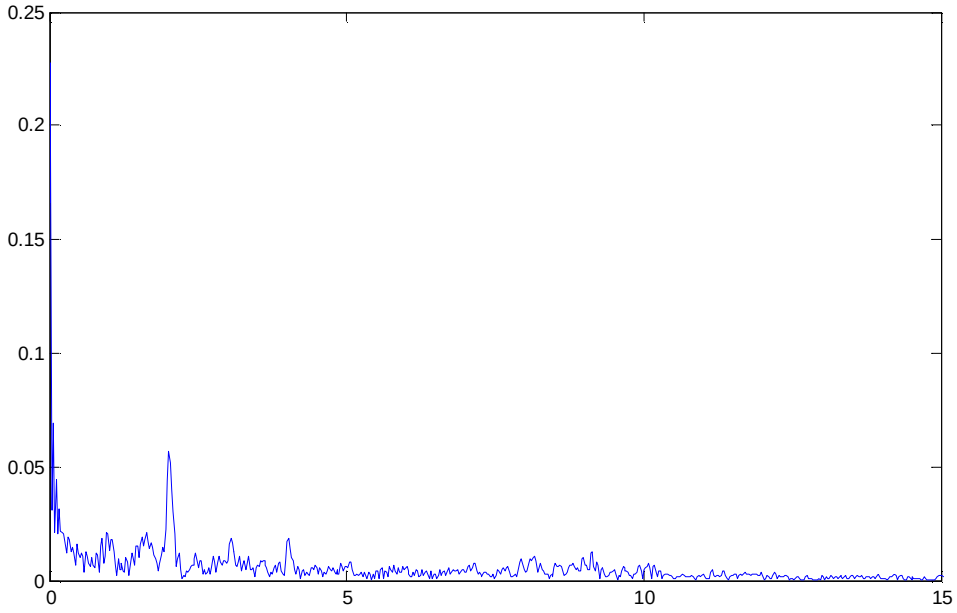

Figure 59:Min+Min iliac

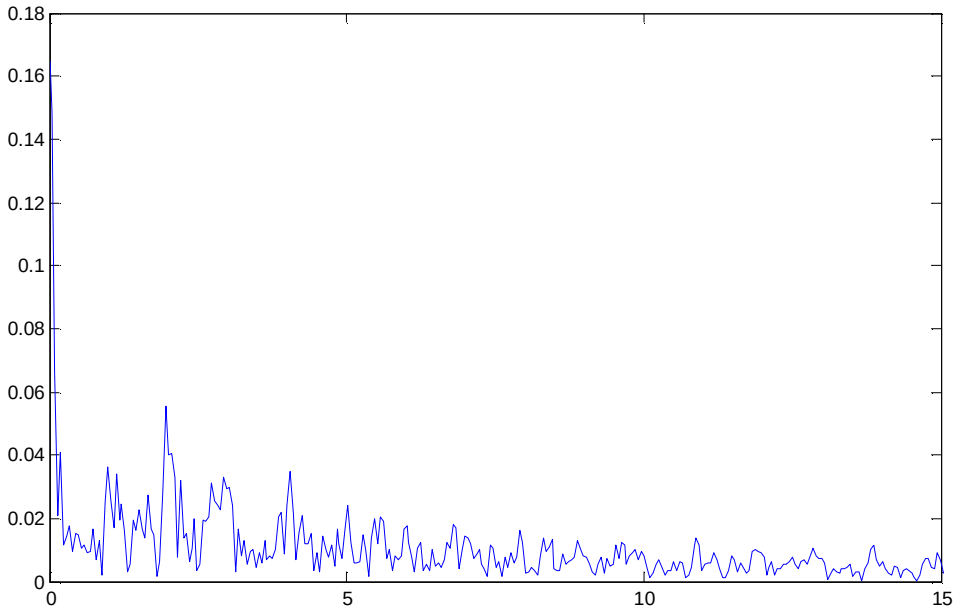

Figure 60: Huge Blockage Iliac

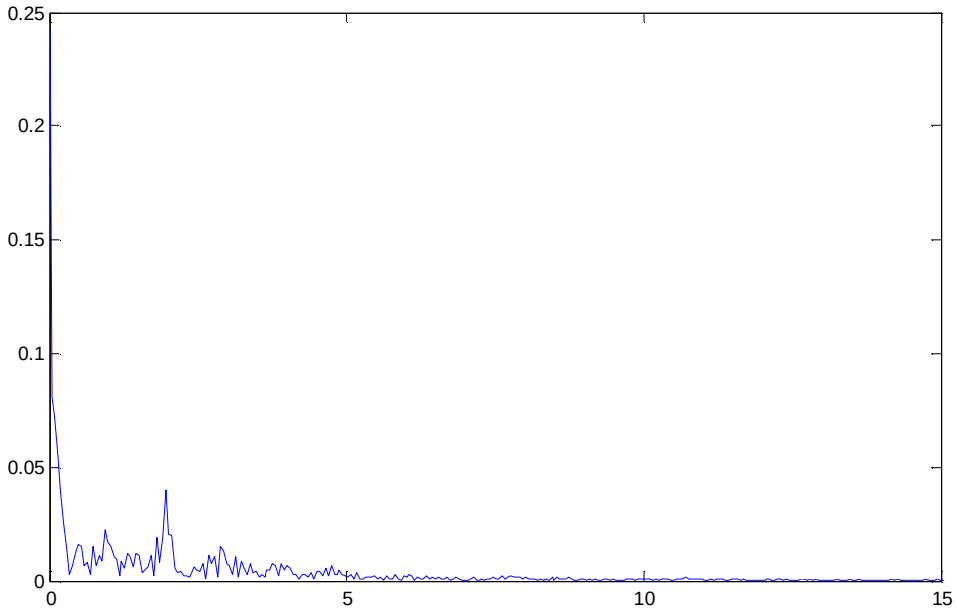

Figure 61: Huge Blockage Abdominal